Electrical Power and Energy Systems 147 (2023) 108882

Contents lists available at ScienceDirect

International Journal of Electrical Power and Energy Systems

journal homepage: www.elsevier.com/locate/ijepes

Asynchronous decentralized adjustable robust operation for multi-area integrated electricity–gas systems considering wind power uncertainty ☆

Junyi Zhai [a], Yuning Jiang [b,*], Xiao Chen [c], Jianing Li [d], Colin N. Jones [b], Xiao-Ping Zhang [e]

[a] College of New Energy, China University of Petroleum (East China), Qingdao Shandong, China
[b] Laboratoire d'Automatique, École Polytechnique Fédérale de Lausanne (EPFL), Lausanne, Switzerland
[c] North China Branch of State Grid Corporation of China, Beijing, China
[d] WSP, Birmingham, United Kingdom
[e] Department of Electronic, Electrical and Systems Engineering, University of Birmingham, Birmingham, United Kingdom

ARTICLE INFO

Keywords:
Multi-area integrated electricity and natural gas system (IEGS)
Wind energy uncertainty
Asynchronous decentralized optimization
Linear decision rules (LDRs)
Automatic generation control (AGC)

ABSTRACT

Modern energy infrastructure has evolved into an integrated electricity and natural gas systems (IEGS), which often encompasses multiple geographically-diverse energy areas. This paper focuses on the decentralized adjustable robust operation problem for multi-area IEGS. Existing distributed algorithms usually require synchronization of all area subproblems, which is hard to scale and could result in under-utilization of computation resources due to the heterogeneity of local areas. To address those limitations, this paper proposes an asynchronous alternating direction method of multipliers (ADMM) based decentralized model for multi-area IEGS. This asynchronous decentralized structure only requires local communications and allows each area to perform local updates with information from a subset of but not all neighbors, where the individual areas' subproblems are solved independently and asynchronously. Meanwhile, the linear decision rules (LDRs)-based adjustable robust operation model is tailored to combine with the automatic generation control (AGC) systems to fully exploit its potential in dealing with renewable energy uncertainty. Numerical results illustrate the effectiveness of the proposed method.

1. Introduction

The development of natural gas-fired units (NGUs) tends to closely link the formerly isolated electricity system and natural gas system together and optimize them as an integrated electricity and natural gas system (IEGS). Furthermore, a growing number of interconnections among regional energy systems bring about additional challenges for coordinating energy flow among multiple areas. The intensified interdependency of IEGS has become an important issue in the reliable operation of modern energy systems [1–3].

So far, energy systems are developing towards more integrated operations. The similarity in gas and electricity consumption profiles gives rise to critical mandates for the coordinated operation of IEGS. In [4], the second-order cone (SOC) relaxation-based steady-state gas flow model is proposed and widely used in the operation problem of natural gas system. In [5], a equivalent gas network model that can accurately reflect dynamic interactions of natural gas and electricity systems is proposed. In [6], the multi-timescale coordinated dispatch model for IEGS is presented. However, the above IEGS operation models are operated in a centralized manner, which may cause difficulties for managing the individual area's information diversity and privacy in multi-area settings. Modern interconnected IEGS typically consists of several geographical regional subsystems that correspond to different IEGS operators (IEGSOs). Recently, some distributed operation models for multi-area IEGS are proposed in [1,7,8]. However, the gas linepack effect is not considered in [1,8], and the renewable energy uncertainty is not considered in [1,7]. Given a distributed framework, each local IEGSO can operate independently and collaborate by sharing limited information. Accordingly, each IEGSO keeps proprietary data, including operation states and topological information, confidential without compromising data privacy and decision-making independence.

Various methods have been employed to decompose the multi-area optimization problems, which can be generally classified into

☆ This work was supported in part from the Youth Program of Natural Science Foundation of Jiangsu Province, China (BK20210103), in part from the Fundamental Research Funds for the Central Universities, China (22CX06053A), and in part from the Swiss National Science Foundation, Switzerland under the RISK project (Risk Aware Data Driven Demand Response, grant number 200021 175627).

* Corresponding author.
E-mail addresses: zhaijunyi@upc.edu.cn (J. Zhai), yuning.jiang@epfl.ch (Y. Jiang), soleilchen@126.com (X. Chen), jianing.li@wsp.com (J. Li), colin.jones@epfl.ch (C.N. Jones), X.P.Zhang@bham.ac.uk (X.-P. Zhang).

https://doi.org/10.1016/j.ijepes.2022.108882
Received 1 July 2021; Received in revised form 8 November 2022; Accepted 1 December 2022
Available online 20 December 2022
0142-0615/© 2022 The Author(s). Published by Elsevier Ltd. This is an open access article under the CC BY license (http://creativecommons.org/licenses/by/4.0/).

three types: (1) the Lagrangian relaxation-based approaches such as the analytical target cascading [9,10], alternating direction method of multipliers (ADMM) [1,7,8,11,12] and auxiliary problem principle [13]; (2) the Karush–Kuhn–Tucker conditions-based approaches such as the heterogeneous decomposition algorithm [14] and the optimality condition decomposition algorithm [15]; and (3) the benders decomposition algorithm [16]. In fact, the majority of these methods are developed based on the premise that the workers can solve subproblems synchronously. However, the scale and complexity of subproblems are usually dependent on the system's physical configuration, and therefore are heterogeneous and require different amounts of computation time. In the synchronous setting, all workers need to wait for the slowest worker to finish its computation or communication. This may lead to the under-utilization of both computation and communication resources as some workers remain idle for most of time [17]. To overcome these drawbacks, the recent works [17,18] have generalized the synchronous ADMM to an asynchronous one. In the asynchronous setting, all workers perform their local updates based on the latest available information from a subset of but not all neighbors, which prevents the speedy workers from spending most of the time idling.

Another challenge for the operation of IEGS is how to hedge renewable energy uncertainty. Robust optimization (RO) [9,19–27] is an attractive option. However, the RO models in [9,19–21] need a decomposition algorithm based on a master-subproblem iteration framework, which may demand a considerable computation time at each iteration. When applied to ADMM, there are two disadvantages. Firstly, the calculation burden will be enlarged as the master-subproblem iteration of decomposition algorithm is needed in every ADMM iteration. Secondly, the robust counterpart of the second-stage problem in those of decomposition-based RO models is bilinear and nonconvex. Although this bilinear problem can be either solved by outer approximation method [28] (only local optimality is guaranteed) or rewritten into a MILP using the big-M method [9,20,21], the convergence of ADMM is not guaranteed on nonconvex problem.

Unlike to the decomposition-based robust approach, the linear decision rules (LDRs) [22–27,29] model can provide a slightly conservative, yet single tractable solution to the adjustable robust formulation. Since the robust counterpart of LDRs-based adjustable approach is usually tractable convex problem, LDRs model is more suitable for the application of decentralized optimization. The LDRs have been applied to adjustable robust optimal power flow (OPF) [22–25], residential distributed generation coordination [26], and generation expansion planning [27]. For the LDRs-based adjustable robust OPF problem, the renewable energy uncertainty is expressed through allowable output interval and the automatic generation control (AGC) system is combined with LDRs in [22,23]. However, the AGC participation factors must be predefined, otherwise the resulting model will be nonlinear. If the AGC participation factors are predefined, the solution will be conservative and the potential of AGC units cannot be fully exploited to deal with renewable energy uncertainty. In [24,25], the renewable energy or load uncertainties are expressed through unadjustable bounded intervals, which is quite conservative. Moreover, the renewable energy curtailment situation cannot be handled in this model. In short, the relationship between LDRs and AGC systems has not been thoroughly studied in above literatures, especially when the uncertainties are expressed through bounded intervals in a controllable polyhedral uncertainty set.

Multi-area IEGS becomes a practical need for growing interconnection of regional energy systems. To address those limitations of synchronous ADMM and overcome disadvantages of decomposition-based robust approach when applied to decentralized optimization, this paper proposes a decentralized LDRs-based adjustable robust operation model for multi-area IEGS via asynchronous ADMM. The information privacy and decision-making independence are preserved among different IEGSOs. The LDRs and AGC systems are fully combined, and thus, the potential of AGC systems in dealing with uncertainties is fully exploited. The contributions of this paper are as follows:

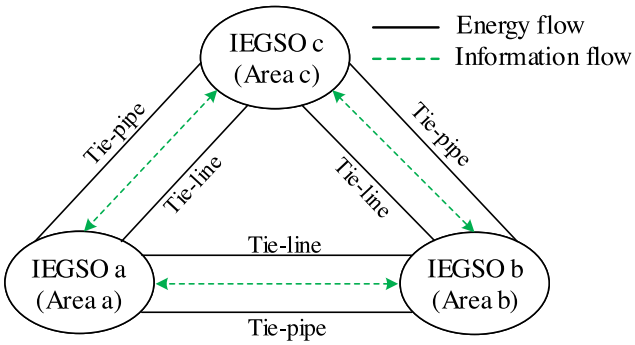

Fig. 1. Structure of decentralized operation in a three-area IEGS.

1. An asynchronous decentralized ADMM for the operation problem of multi-area IEGS is proposed. Different from synchronous ADMM, this asynchronous decentralized structure only requires local communication and allows each area to perform local updates with information from a subset of but not all neighbors. Each IEGSO can operate their respective systems independently and asynchronously with the consideration that only limited information is shared with each other. The computational bottleneck arising from slower subproblems can be eliminated, which minimizes the idle time and improves the computational efficiency.
2. The LDRs-based adjustable robust extension of asynchronous ADMM capable of handling uncertainties is proposed. LDRs are utilized to recast the regional adjustable robust operation problem as a computationally tractable SOCP problem. This LDRs model can reduce the computation burden of every ADMM iteration and guarantee the convergence of asynchronous ADMM.
3. Different from [22,23] that predefine the AGC participation factors, this paper tailors the LDRs model to combine with the AGC systems and treats participation factors as optimizable variables to fully exploit its potential in dealing with uncertainties. Meanwhile, different from LDRs models in [24,25] that express uncertainties using unadjustable bounded intervals, this paper adopts the bounded intervals in a controllable polyhedral uncertainty set, leading to significantly less conservative and more practical solutions.

This paper is organized as follows. Section 2 presents the decomposition of multi-area IEGS. Section 3 addresses the adjustable robust operation model of single area. Section 4 proposes the decentralized adjustable robust algorithm. Case study and conclusion are presented in Sections 5 and 6. Appendix is given after Section 6.

Notation: Boldface lower case and upper case letters represent vectors and matrices, respectively. A constraint is called semi-infinite if it can be formulated as $\forall w \in \mathcal{W},\ f(x,w) \le 0$ with set $\mathcal{W}$ and a function f parametrized over w.

2. Decomposition of Multi-area IEGS

This paper considers partitioning an IEGS into multiple areas. In practice, this allows to design a decentralized decision-making scheme, in which each area is operated locally while cooperating with its neighbors by sharing a limited set of data. As a result, proprietary data, for example, operation states and topological information, can be kept confidential in each area. Moreover, each area does not require global knowledge of the entire system structure. Fig. 1 shows an example of three-area interconnected IEGS for illustration.

For a given multi-area IEGS, we denote by set $\mathcal{R}$ to enumerate all areas based on the partitioning, set $\mathcal{T}$ to represent all time periods. For area $a \in \mathcal{R}$, we consider a wind-integrated electricity network

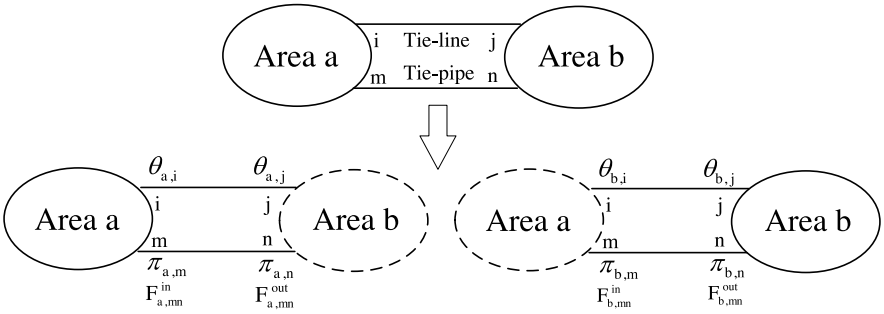

Fig. 2. Decomposition strategy of a two-area IEGS.

denoted by the tuple $(\mathcal{B}_a, \mathcal{L}_a, \mathcal{NG}_a, \mathcal{G}_a, \mathcal{W}_a)$, where $\mathcal{B}_a$ denotes the set of buses, $\mathcal{L}_a \subseteq \mathcal{B}_a \times \mathcal{B}_a$ the set of power lines, $\mathcal{NG}_a \subseteq \mathcal{B}_a$ the set of NGUs, $\mathcal{G}_a \subseteq \mathcal{B}_a$ the set of NGUs and non-NGUs, and $\mathcal{W}_a \subseteq \mathcal{B}_a$ the set of wind farms. Similarly, the gas system is denoted by the tuple $(\mathcal{N}_a, \mathcal{GP}_a, \mathcal{GW}_a, \mathcal{GS}_a, \mathcal{GC}_a)$, where $\mathcal{N}_a$ denotes the set of nodes, $\mathcal{GP}_a \subseteq \mathcal{N}_a \times \mathcal{N}_a$ the set of pipelines, $\mathcal{GW}_a \subseteq \mathcal{N}_a$ the set of gas wells, $\mathcal{GS}_a \subseteq \mathcal{N}_a$ the set of gas storages, and $\mathcal{GC}_a \subseteq \mathcal{N}_a$ the set of compressors.

Operating a multi-area IEGS in a decentralized way requires to find proper couplings between the neighboring areas. In this paper, the phase angle of boundary bus on tie-line, the pressure of boundary node on tie-pipe, and the natural gas flow of tie-pipe are selected as coupling variables. For any two connected areas, there are one power tie-line at boundary buses i and j and one gas tie-pipe at boundary nodes m and n as shown in Fig. 2. Throughout this paper, we use notations $\mathcal{P}$ to denote the neighboring ares, i.e., $(a, b) \in \mathcal{P} \subseteq \mathcal{R} \times \mathcal{R}$ in Fig. 2, and $\mathcal{L}^c$ to denote the corresponding connecting tie-line, i.e., $(i, j) \in \mathcal{L}^c$ in Fig. 2, and $\mathcal{GP}^c$ to denote the corresponding connecting tie-pipe, i.e., $(m, n) \in \mathcal{GP}^c$ in Fig. 2.

For the electricity part in each area $a \in \mathcal{R}$, the set of buses $\mathcal{B}_a = \mathcal{B}_a^o \cup \mathcal{B}_a^v$ is separated as the physical buses $\mathcal{B}_a^o$ according to the partitioning, and the virtual buses $\mathcal{B}_a^v$ on the boundary. If areas a and b are connected via tie-line $(i, j) \in \mathcal{L}^c$, we introduce two virtual buses for areas a and b (see Fig. 2) described by voltage angle $\theta_{a,j}$ and $\theta_{b,i}$, respectively. Then, we introduce the consensus constraint

$$\theta_{a,it} = \theta_{b,it}\ ,\ \theta_{a,jt} = \theta_{b,jt} \tag{1}$$

to state that the voltage angles of an end bus perceived by its connected areas should be identical. Similarly, for the gas system in each area $a \in \mathcal{R}$, the set of nodes $\mathcal{N}_a = \mathcal{N}_a^o \cup \mathcal{N}_a^v$ is separated as the physical nodes $\mathcal{N}_a^o$ according to the partitioning, and the virtual nodes $\mathcal{N}_a^v$ on the boundary. If areas a and b are connected via tie-pipe $(m, n) \in \mathcal{GP}^c$, we introduce two virtual nodes for areas a and b (see Fig. 2) described by node pressure $\pi_{a,n}$ and $\pi_{b,m}$, respectively. Then, we introduce the consensus constraint

$$\pi_{a,mt} = \pi_{b,mt}\ ,\ \pi_{a,nt} = \pi_{b,nt} \tag{2}$$

to state that the pressures of an end node perceived by its connected areas should be identical, and

$$F_{a,mnt}^{in} = F_{b,mnt}^{in}\ ,\ F_{a,mnt}^{out} = F_{b,mnt}^{out} \tag{3}$$

to state that the gas flow along tie-pipe perceived by its connected areas should be identical.

3. Adjustable robust operation model of single area

This section introduces the regional adjustable robust operation formulation for each area.

3.1. Local objective function

The local objective of each area is to minimize the total operation cost given by

$$M_a = \sum_{t\in\mathcal{T}} \Bigg\{ \sum_{g\in\mathcal{G}_a\setminus\mathcal{NG}_a} \left[c_{1g}\left(\hat{P}_{gt}^G\right)^2 + c_{2g}\hat{P}_{gt}^G + c_{3g} \right] + \sum_{w\in\mathcal{GW}_a} p_w^W F_{wt}^W + \sum_{s\in\mathcal{GS}_a} p_s^S \left(F_{st}^{S,out} + F_{st}^{S,in} \right) \Bigg\} \tag{4}$$

including the generating cost of non-NGUs, the gas production cost of gas wells, and the operating cost of gas storages in the area, where c_{1g}, c_{2g}, and c_{3g} denote the fuel cost coefficients of unit g, $\hat{P}_{gt}^G$ the reference base-point output of unit g at time t in the nominal scenario, p_w^W the gas production cost of gas well w, p_s^S the operation cost of gas storage s, F_{wt}^W the output of gas well w at time t, $F_{st}^{s,in}$ and $F_{st}^{s,out}$ denote the storing/releasing rate of gas storage s at time t, respectively.

3.2. Constraints of local electricity system

We describe the randomness of wind farm output by

$$\forall\, i \in \mathcal{W}_a\ ,\forall\, t \in \mathcal{T},\ \ \tilde{P}_{it}^W = \overline{P}_{it}^W + \Delta P_{it}^W z_{it}\ , \tag{5}$$

where $\tilde{P}_{it}^W$, $\overline{P}_{it}^W$, and ΔP_{it}^W are the uncertain output, forecasted output, and the maximum magnitude of deviation from forecast output of wind farm i at time t, respectively. Auxiliary variable z_{it} denotes the upward/downward deviation from the forecasts subject to $\boldsymbol{z} = \{z_{it}\}_{i\in\mathcal{W}_a, t\in\mathcal{T}} \in \mathcal{Z}_a \subseteq \mathbb{R}^{|\mathcal{W}_a|\times|\mathcal{T}|}$. Here, the controllable polyhedral uncertainty set $\mathcal{Z}_a = \left\{ \boldsymbol{z} \in \mathbb{R}^{|\mathcal{W}_a|\times|\mathcal{T}|} \,\middle|\, |z_{it}| \le 1\ ,\ \sigma_a \ge \sum_{i\in\mathcal{W}_a} |z_{it}| \right\}$ is equivalent to

$$\mathcal{Z}_a = \left\{ \boldsymbol{z} \in \mathbb{R}^{|\mathcal{W}_a|\times|\mathcal{T}|} \,\middle|\, \begin{array}{l} \exists z_{it}^+, z_{it}^- \in [0,1], k \in \mathcal{W}_a, t \in \mathcal{T}\ : \\ z_{it} = z_{it}^+ - z_{it}^-, z_{it}^+ + z_{it}^- \le 1 \\ \sum\limits_{i\in\mathcal{W}_a} z_{it}^+ + z_{it}^- \le \sigma_a \end{array} \right\} \tag{6}$$

Remark 1. The choice of σ_a in $\mathcal{Z}_a$ aims at adjusting the conservativeness of the robust solution. $\sigma_a = 0$ results in deterministic representation, $\sigma_a > 0$ leads to uncertain parameters, which could deviate from the forecast values. Specifically, $\sigma_a = \left|\mathcal{W}_a\right|$ degenerates into the unadjustable bounded interval in [24,25].

Based on LDRs, we define adjustable robust unit output and wind farm output by

$$\begin{aligned} P_{it}^G &= \hat{P}_{it}^G - \alpha_{it} \sum_{k\in\mathcal{W}_a} \left(\tilde{P}_{kt}^W - \overline{P}_{kt}^W \right) \\ &= \hat{P}_{it}^G - \alpha_{it} \sum_{k\in\mathcal{W}_a} \Delta P_{kt}^W z_{kt}\ , \qquad i \in \mathcal{G}_a\ , a \in \mathcal{R}\ , t \in \mathcal{T} \end{aligned} \tag{7a}$$

$$1 = \sum_{i\in\mathcal{G}_a} \alpha_{it} \ \text{ with } \ \alpha_{gt} \in [0,1], \qquad i \in \mathcal{G}_a, a \in \mathcal{R}, t \in \mathcal{T} \tag{7b}$$

$$\begin{aligned} P_{jt}^W &= \hat{P}_{jt}^W - \sum_{k\in\mathcal{W}_a} \beta_{jkt}\left(\tilde{P}_{kt}^W - \overline{P}_{kt}^W\right) \\ &= \hat{P}_{jt}^W - \sum_{k\in\mathcal{W}_a} \beta_{jkt}\left(\Delta P_{kt}^W z_{kt}\right), \qquad j \in \mathcal{W}_a,\ a \in \mathcal{R},\ t \in \mathcal{T} \end{aligned} \tag{7c}$$

where P_{gt}^G and P_{it}^W respectively denote the output from unit g and wind farm i at time t under the realization of wind generation, $\hat{P}_{jt}^W$ denotes the reference base-point output of wind farm j at time t in the nominal scenario, β_{jkt} and α_{gt} denote the adjustable terms under the realization of wind generation, and α_{gt} is directly compatible with the unit participation factors of AGC systems.

Remark 2. Different from [22,23], this paper treats AGC participation factors as optimizable variables. The resulting LDRs model is directly compatible with AGC systems where generators respond to area control error (ACE) according to the optimized participation factors.

Note that the bus voltage angle under the realization of wind generation can also be divided into two components, the non-adjustable component that is associated with the nominal scenario and the adjustable component that varies with the uncertain wind forecast errors as follows. Detailed derivation can be seen in Appendix.

$$\theta_{it} = \hat{\theta}_{it} - \sum_{k\in\mathcal{W}_a}\left(\tilde{B}_{ik}\beta_{ikt} + \sum_{g\in\mathcal{G}_a}\tilde{B}_{ig}\alpha_{gt}\right)\left(\tilde{P}_{kt}^W - \overline{P}_{kt}^W\right) \tag{8}$$

where θ_{it} denotes the phase angle of bus i at time t under the realization of wind generation, $\hat{\theta}_{it}$ denotes the reference base-point of phase angle of bus i at time t in the nominal scenario, $\tilde{B}_{ik}$ denotes the element of electricity network admittance inverse matrix, with the reference angle at bus 1.

Accordingly, the typical constraints of local electricity system in each area is summarized as follows,

$$\hat{P}_{it}^G = 0, \qquad i \in \mathcal{B}_a^o \backslash \mathcal{G}_a,\ a \in \mathcal{R},\ t \in \mathcal{T} \tag{9a}$$

$$\hat{P}_{it}^W = 0, \qquad i \in \mathcal{B}_a^o \backslash \mathcal{W}_a,\ a \in \mathcal{R},\ t \in \mathcal{T} \tag{9b}$$

$$\hat{P}_{it}^G + \hat{P}_{it}^W - \sum_{j\in\Phi_i}\frac{\hat{\theta}_{it} - \hat{\theta}_{jt}}{x_{ij}} = P_{it}^D, \qquad i \in \mathcal{B}_a^o,\ a \in \mathcal{R},\ t \in \mathcal{T} \tag{9c}$$

$$0 \le P_{it}^W \le \tilde{P}_{it}^W \quad \text{with (5) and (7c)} \ \forall z \in \mathcal{Z}_a \qquad i \in \mathcal{W}_a,\ a \in \mathcal{R},\ t \in \mathcal{T} \tag{9d}$$

$$\underline{P}_{it}^G \le P_{it}^G \le \overline{P}_i^G \quad \text{with (5), (7a) and (7b)} \ \forall z \in \mathcal{Z}_a \qquad i \in \mathcal{G}_a,\ a \in \mathcal{R},\ t \in \mathcal{T} \tag{9e}$$

$$-R_i^D \le P_{it}^G - P_{it-1}^G \le R_i^U \quad \text{with (5), (7a) and (7b)} \ \forall z \in \mathcal{Z}_a \qquad i \in \mathcal{G}_a,\ a \in \mathcal{R},\ t \in \mathcal{T}\backslash\{1\} \tag{9f}$$

$$-\overline{L}_{ij} \le \frac{\theta_{it} - \theta_{jt}}{x_{ij}} \le \overline{L}_{ij} \quad \text{with (5), (7b), and (8)} \ \forall z \in \mathcal{Z}_a \qquad (i,j) \in \mathcal{L}_a,\ a \in \mathcal{R},\ t \in \mathcal{T} \tag{9g}$$

$$\theta_{1t}^{\text{ref}} = 0, \qquad t \in \mathcal{T} \tag{9h}$$

with Φ_i the neighboring buses of bus i, R_i^U and R_i^D respectively denote the maximum upward and downward ramping rates of unit i, P_{it}^D denotes the load demand at bus i at time t, x_{ij} and $\overline{L}_{ij}$ denote the reactance and capacity of transmission line $(i,j) \in \mathcal{L}_a$, respectively, $\underline{P}_i^G$ and $\overline{P}_i^G$ denote the minimum and maximum output for all $i \in \mathcal{G}_a$, respectively.

Constraints (9a)–(9c) denote the bus power balance in the nominal scenario represented by DC power flow model while (9d)–(9h) denote the constraints under the realization of wind generation, where (9d) is the wind farm output limit, (9e) is the unit output limit, (9f) is the unit ramping rate limit, (9g) is the capacity limit of transmission line, (9h) defines bus 1 as the reference bus of the entire system.

3.3. Constraints of local natural gas system

The typical constraints of local natural gas system in each area describing the quasi-steady-state operating characteristics with linepack gas model are

$$\begin{aligned} &\sum_{w\in\Psi_m^W} F_{wt}^W + \sum_{s\in\Psi_m^S}\left(F_{st}^{S,out} - F_{st}^{S,in}\right) + \sum_{n\in\Psi_m}\left(F_{mnt}^{out} - F_{mnt}^{in}\right) \\ &= \sum_{i\in\Psi_m^G} F_{it}^G + \sum_{d\in\Psi_m^D} F_{dt}^D \\ &+ \sum_{k\in\Psi_m^C}\tau_{kt}^C + \sum_{k\in\Psi_m^C} F_{kt}^C, \qquad m \in \mathcal{N}_a^o,\ a \in \mathcal{R},\ t \in \mathcal{T} \end{aligned} \tag{10a}$$

$$\underline{F}_w^W \le F_{wt}^W \le \overline{F}_w^W, \qquad w \in \mathcal{GW}_a,\ a \in \mathcal{R},\ t \in \mathcal{T} \tag{10b}$$

$$0 \le F_{st}^{S,out} \le \overline{F}_s^{S,out}, \qquad s \in \mathcal{GS}_a,\ a \in \mathcal{R},\ t \in \mathcal{T} \tag{10c}$$

$$0 \le F_{st}^{S,in} \le \overline{F}_s^{S,in}, \qquad s \in \mathcal{GS}_a,\ a \in \mathcal{R},\ t \in \mathcal{T} \tag{10d}$$

$$E_{st}^S = E_{st-1}^S + F_{st}^{S,in} - F_{st}^{S,out}, \qquad s \in \mathcal{GS}_a,\ a \in \mathcal{R},\ t \in \mathcal{T} \tag{10e}$$

$$\underline{E}_s^S \le E_{st}^S \le \overline{E}_s^S, \qquad s \in \mathcal{GS}_a,\ a \in \mathcal{R},\ t \in \mathcal{T} \tag{10f}$$

$$F_{mnt} = C_{mn}\sqrt{\pi_{mt}^2 - \pi_{nt}^2}, \qquad (m,n) \in \mathcal{GP}_a,\ a \in \mathcal{R},\ t \in \mathcal{T} \tag{10g}$$

$$F_{mnt} = \left(F_{mnt}^{out} + F_{mnt}^{in}\right)/2, \qquad (m,n) \in \mathcal{GP}_a,\ a \in \mathcal{R},\ t \in \mathcal{T} \tag{10h}$$

$$F_{mnt}^{LP} = K_{mn}\left(\pi_{nt} + \pi_{mt}\right)/2, \qquad (m,n) \in \mathcal{GP}_a,\ a \in \mathcal{R},\ t \in \mathcal{T} \tag{10i}$$

$$F_{mnt}^{LP} = F_{mnt-1}^{LP} + F_{mnt}^{in} - F_{mnt}^{out}, \qquad (m,n) \in \mathcal{GP}_a,\ a \in \mathcal{R},\ t \in \mathcal{T} \tag{10j}$$

$$F_{mnt}^{in}, F_{mnt}^{out} \ge 0, \qquad (m,n) \in \mathcal{GP}_a,\ a \in \mathcal{R},\ t \in \mathcal{T} \tag{10k}$$

$$\pi_{nt} \le \pi_{mt}, \qquad (m,n) \in \mathcal{GP}_a,\ a \in \mathcal{R},\ t \in \mathcal{T} \tag{10l}$$

$$\underline{\pi}_m \le \pi_{mt} \le \overline{\pi}_m, \qquad m \in \mathcal{N}_a^o,\ a \in \mathcal{R},\ t \in \mathcal{T} \tag{10m}$$

$$0 \le F_{mnt} \le \overline{F}_{mn}, \qquad (m,n) \in \mathcal{GP}_a,\ a \in \mathcal{R},\ t \in \mathcal{T} \tag{10n}$$

$$0 \le F_{kt}^C \le \overline{F}_k^C, \qquad k \in \mathcal{GC}_a,\ a \in \mathcal{R},\ t \in \mathcal{T} \tag{10o}$$

$$\tau_{kt}^C = \gamma_k F_{kt}^C, \qquad k \in \mathcal{GC}_a,\ a \in \mathcal{R},\ t \in \mathcal{T} \tag{10p}$$

$$\underline{r}_k \le \pi_{kt}^{out}/\pi_{kt}^{in} \le \bar{r}_k, \qquad k \in \mathcal{GC}_a,\ a \in \mathcal{R},\ t \in \mathcal{T} \tag{10q}$$

$$F_{it}^G = \omega_g P_{gt}^G \quad \text{with (5), (7a), and (7b)} \ \forall z \in \mathcal{Z}_a \qquad (i,g) \in \Omega_a,\ a \in \mathcal{R},\ t \in \mathcal{T} \tag{10r}$$

with Ψ_m, Ψ_m^W, Ψ_m^S, Ψ_m^G, Ψ_m^D, and Ψ_m^C the set of gas nodes, gas wells, gas storages, NGUs, gas loads, and compressors connected to node m, F_{dt}^D the gas demand of node d at time t, π_{mt} the gas pressure of node m at time t, E_{st}^S the volume of gas storage s at time t, $\overline{F}_s^{in}$ and $\overline{F}_s^{out}$ denote the maximum storing and releasing rate of gas storage s, respectively, $[\underline{\pi}_m, \overline{\pi}_m]$ the interval of π_{mt}, $[\underline{F}_w^W, \overline{F}_w^W]$ the interval of F_{wt}^W, $[\underline{F}_s^S, \overline{F}_s^S]$ the interval of F_{st}^S, $[\underline{r}_k, \bar{r}_k]$ the interval of compression ratio of compressor k, $[\underline{E}_s^S, \overline{E}_s^S]$ the interval of E_{st}^S, F_{gt}^G the gas consumption of NGU g at time t, F_{kt}^C the gas flow through compressor k at time t, F_{mnt}^{in} and F_{mnt}^{out} denote the inflow and outflow of pipeline mn at time t, respectively, F_{mnt} and F_{mnt}^{LP} denote the average gas flow and linepack of pipeline mn at time t, respectively, $\overline{F}_k^C$ and $\overline{F}_{mn}$ denote the maximum gas flow through compressor k and pipeline mn, C_{mn} and K_{mn} denote the Weymouth constant and linepack constant of pipeline mn, respectively, τ_{kt}^C the gas consumption of compressor k at time t, γ_k the efficiency of compressor k, Ω_a denotes the pairs of node $i \in \mathcal{N}_a^o$ and its equipped NGU $g \in \mathcal{NG}_a$, ω_g the conversion coefficient of NGU g.

Eq. (10a) represents the nodal gas flow balance. Eq. (10b) represents the output limit of gas wells. Eqs. (10c)–(10f) represent the output limit of gas storages. Eqs. (10g)–(10h) describe the steady-state Weymouth gas flow model [4,30] denoted by the nodal gas pressure and pipeline gas flow. According to the gas-transmission-system operation practice, the gas flow direction does not change intra-day [31]. Thus, it is a reasonable assumption in short-term operation problem, whereas the long-term operation or planning decision should consider bi-directional natural gas flows. Eqs. (10i)–(10k) represent the gas linepack limit,

which is considered as proportional to the average gas pressure and the pipeline characteristics. Since the real-time gas load uncertainties can be practically balanced by linepack, the uncertainties of gas loads are not considered here. Constraints (10l)–(10m) denote the nodal pressure. Constraint (10n) and (10o) represent the transmission capacity of gas pipelines and compressors, respectively. For gas compressors, their gas consumptions represent a specified percentage (typically 3%–5%) [32] of the transported gas flow as given in (10p), while (10q) denotes the compression ratio limit of outlet and inlet gas pressures. The gas consumption of the ith NGU in the electricity network is fed by gas extracted from the mth gas node in the gas network. Eq. (10r) assumes a linear relationship [33,34] between the gas consumption of NGUs and their power outputs under the realization of wind power generation, which ensures the safe operation of the gas system under wind power uncertainty.

Constraint (10g) is nonconvex, we apply SOC relaxation as discussed in [4] to deal with its nonconvexity. In a result, we have convex SOC constraints derived by

$$\begin{aligned} F_{mnt} =& C_{mn}\sqrt{\pi_{mt}^2-\pi_{nt}^2} \;\rightarrow F_{mnt}^2/C_{mn}^2=\pi_{mt}^2-\pi_{nt}^2 \\ \rightarrow& F_{mnt}^2/C_{mn}^2+\pi_{nt}^2\le\pi_{mt}^2 \rightarrow \left\|\begin{bmatrix} F_{mnt}/C_{mn} \\ \pi_{nt}\end{bmatrix}\right\|_2 \le \pi_{mt}\,. \end{aligned} \tag{11}$$

If the solution satisfies (10g), the relaxation is exact and the solution is globally optimal. However, the relaxation (11) may not always be exact during the iteration of optimization algorithm. To drive the exactness of SOC relaxation, an additional penalty term

$$M_a' = \sum_{t\in\mathcal{T}}\sum_{(m,n)\in\mathcal{G}\mathcal{P}_a} \beta\left(\pi_{mt}-\pi_{nt}\right),$$

with smaller positive constant β is added to the objective function, which drives the $\pi_{mt}^2-\pi_{nt}^2$ towards F_{mnt}^2/C_{mn}^2 [35,36]. This positive linear penalty term makes the violation of the constraint (10g) smaller.

Remark 3. The semi-infinite constraints (9d)–(9g) and (10r) are robust for any realization of wind generation in the controllable polyhedral uncertainty set.

4. Decentralized adjustable robust algorithm

This section first proposes a decentralized LDRs-based adjustable robust operation formulation. Then, we discuss how to solve the problem by using the standard synchronous ADMM in a decentralized manner. Moreover, an asynchronous ADMM based decentralized method is presented to reduce the impact of time delay between neighbors.

4.1. Decentralized LDRs-based adjustable robust formulation

We stack by $\chi_a = \left(\{\theta_{it}\}_{i\in\mathcal{B}_a,t\in\mathcal{T}},\{P_{it}^G\}_{i\in\mathcal{G}_a,t\in\mathcal{T}},\{P_{it}^W\}_{i\in\mathcal{W}_a,t\in\mathcal{T}}\right)$ the decision variables of regional IEGS under the realization of wind generation and introduce the LDRs

$$\chi_a = \hat{\chi}_a + \boldsymbol{U}_a\boldsymbol{z}\,,\ \boldsymbol{U}_a\in\mathcal{U}_a\,,\ \boldsymbol{z}\in\mathcal{Z}_a \tag{12}$$

to deal with the semi-infinite constraints (9d)–(9g) and (10r), where $\hat{\chi}_a$ and $\boldsymbol{U}_a$ denote the non-adjustable term in the nominal scenario and adjustable term due to the uncertainties, respectively. Then, we write down (9d)–(9g) and (10r) and into the worst-case dense form

$$\max_{\boldsymbol{z}\in\mathcal{Z}_a}\ \boldsymbol{W}_a(\hat{\chi}_a+\boldsymbol{U}_a\boldsymbol{z})\le\nu_a\,. \tag{13}$$

Writing the dual equivalent form of the inner maximization problem leads to

$$(\chi_a,\zeta_a)\in\mathcal{X}_a^E, \tag{14}$$

where ζ_a denotes the associated dual variables of constraints $\boldsymbol{z}\in\mathcal{Z}_a$, $\mathcal{X}_a^E$ is a polyhedral constraint set. The derivation from (13) to (14) in details can be found in Appendix. Finally, we obtain the LDRs-based adjustable robust operation model for multi-area IEGS as follows.

$$\min\ \sum_{a\in\mathcal{R}}\left(M_a+M_a'\right) \tag{15a}$$

s.t. (9a)–(9c),(9h), (10a)–(10f), (10h)–(10q),

(11), (27), (28), (29), (30), (40), (41), (44), (45), (48). (15b)

The above convex model aims at minimizing the base-case operation cost in nominal scenario over linear and SOC constraints, while adaptively and securely adjusting the output of AGC units in response to possible realizations of wind power uncertainties. The proposed model does not need any decomposition-based robust algorithm and can be directly solved by commercial solvers. Noted that some of these constraints are shown in Appendix.

Moreover, we use notation $\boldsymbol{x}_a$ to stack all local variables w.r.t area a and $\mathcal{X}_a$ to collect all regional constraints (15b). Accordingly, the multi-area adjustable robust operation problem can be written in the decentralized form

$$\min_{\boldsymbol{x}}\ \sum_{a\in\mathcal{R}} f_a(\boldsymbol{x}_a) \tag{16a}$$

$$\text{s.t.}\quad \boldsymbol{A}_{a,b}\boldsymbol{x}_a=\boldsymbol{A}_{b,a}\boldsymbol{x}_b\,,\ (a,b)\in\mathcal{P} \tag{16b}$$

$$\boldsymbol{x}_a\in\mathcal{X}_a\,,\ a\in\mathcal{R}. \tag{16c}$$

Here, f_a is given by the regional objective (15a), the coupled affine equality constraint (16b) summarizes constraints (1), (2) and (3) for all $(a,b)\in\mathcal{P}$, where the selection matrices $\mathbf{A}_{a,b}$ are diagonal whose diagonal element is either 1 or 0.

4.2. Synchronous ADMM for decentralized operation

In order to solve (16) using ADMM, we introduce consensus variables $\boldsymbol{y}$ and the following affine equalities

$$\boldsymbol{A}_{a,b}\boldsymbol{x}_a=\boldsymbol{y}_{a,b}\,,\ \boldsymbol{A}_{b,a}\boldsymbol{x}_b=\boldsymbol{y}_{a,b}\,,\ (a,b)\in\mathcal{P} \tag{17}$$

where $\boldsymbol{y}_{a,b}$ includes the elements of $\boldsymbol{y}$ w.r.t. the coupling between areas a and b. Then, we stack all local consensus variables into the compact form

$$\boldsymbol{A}_a\boldsymbol{x}_a=\boldsymbol{y}_a\,,\ a\in\mathcal{R} \tag{18}$$

with selection matrices $\boldsymbol{A}_a$, $a\in\mathcal{R}$. In a result, the augmented Lagrangian is written as

$$L(\boldsymbol{x},\boldsymbol{y},\lambda)=\sum_{a\in\mathcal{R}}\left\{f_a(\boldsymbol{x}_a)+\lambda_a^{\top}\left(\boldsymbol{A}_a\boldsymbol{x}_a-\boldsymbol{y}_a\right)+\frac{1}{2}\left\|\boldsymbol{A}_a\boldsymbol{x}_a-\boldsymbol{y}_a\right\|_{\Sigma_a}^2\right\},$$

where λ_a denotes the Lagrangian multipliers of (18), diagonal matrices $\Sigma_a\succ 0$ introduce the parameters of penalty term in row-wise, i.e.,

$$\frac{1}{2}\left\|\boldsymbol{A}_a\boldsymbol{x}_a-\boldsymbol{y}_a\right\|_{\Sigma_a}^2=\frac{1}{2}\left(\boldsymbol{A}_a\boldsymbol{x}_a-\boldsymbol{y}_a\right)^{\top}\Sigma_a\left(\boldsymbol{A}_a\boldsymbol{x}_a-\boldsymbol{y}_a\right),$$

which follows the fact that matrices $\boldsymbol{A}_a$ are selection matrices. The synchronous ADMM iteration is thus, given by

$$\boldsymbol{x}_a^{\ell+1}=\underset{\boldsymbol{x}_a\in\mathcal{X}_a}{\operatorname{argmin}}\ f_a(\boldsymbol{x}_a)+\lambda_a^{\ell\top}\left(\boldsymbol{A}_a\boldsymbol{x}_a-\boldsymbol{y}_a^{\ell}\right)+\frac{1}{2}\left\|\boldsymbol{A}_a\boldsymbol{x}_a-\boldsymbol{y}_a^{\ell}\right\|_{\Sigma_a}^2\,,\ a\in\mathcal{R} \tag{19a}$$

$$\lambda_a^{\ell+1}=\lambda_a^{\ell}+\Sigma_a(\boldsymbol{A}_a\boldsymbol{x}_a^{\ell+1}-\boldsymbol{y}_a^{\ell})\,,\ a\in\mathcal{R} \tag{19b}$$

$$\begin{aligned}\boldsymbol{y}_{a,b}^{\ell+1}=&\underset{\boldsymbol{y}_{a,b}}{\operatorname{argmin}}(\boldsymbol{A}_{a,b}\boldsymbol{x}_a^{\ell+1}-\boldsymbol{y}_{a,b})^{\top}\lambda_{a,b}^{\ell+1}+\frac{1}{2}\left\|\boldsymbol{A}_{a,b}\boldsymbol{x}_a^{\ell+1}-\boldsymbol{y}_{a,b}\right\|_{\Sigma_a}^2 \\ &+(\boldsymbol{A}_{b,a}\boldsymbol{x}_b^{\ell+1}-\boldsymbol{y}_{a,b})^{\top}\lambda_{b,a}^{\ell+1}+\frac{1}{2}\left\|\boldsymbol{A}_{b,a}\boldsymbol{x}_b^{\ell+1}-\boldsymbol{y}_{a,b}\right\|_{\Sigma_b}^2 \end{aligned} \tag{19c}$$

$$=\left(\Sigma_a+\Sigma_b\right)^{-1}\left(\Sigma_a\boldsymbol{A}_{b,a}\boldsymbol{x}_b^{\ell+1}+\Sigma_b\boldsymbol{A}_{a,b}\boldsymbol{x}_a^{\ell+1}-\lambda_{a,b}^{\ell+1}-\lambda_{b,a}^{\ell+1}\right),\ (a,b)\in\mathcal{P}. \tag{19d}$$

Here, ℓ denotes a global iteration counter. The local primal update (19a) and dual update (19b) can be employed in parallel while the

consensus update (19d) can be proceed either by areas a or b. The entire algorithm is fully decentralized requiring only neighbor-to-neighbor communication. However, step (19d) needs the information from both areas a and b, which in practice, easily encounters a delay at each iteration as areas a and b might spend different time in executing (19a) and (19b) due to local heterogeneity. To overcome this drawback, the next section introduces an asynchronous ADMM based decentralized algorithm to solve (16).

4.3. Asynchronous ADMM for decentralized operation

Algorithm 1 Asynchronous ADMM in area a

Initialization:

- choose λ_a^0, set $\ell_a = 0$;
- solve local problem $\boldsymbol{x}_a^0 = \underset{\boldsymbol{x}_a \in \mathcal{X}_a}{\operatorname{argmin}} \ f_a(\boldsymbol{x}_a)$;
- send $(\boldsymbol{A}_{a,b}\boldsymbol{x}_a^0, \lambda_{a,b}^0)$ to all neighbors $b \in \mathcal{R}_a$.

Repeat:

1. Update primal by

$$\boldsymbol{x}_a^{\ell_a+1} = \underset{\boldsymbol{x}_a \in \mathcal{X}_a}{\operatorname{argmin}} \ f_a(\boldsymbol{x}_a) + \left(\boldsymbol{A}_a\boldsymbol{x}_a\right)^\top \lambda_a^{\ell_a} + \frac{1}{2}\left\|\boldsymbol{A}_a\boldsymbol{x}_a - \boldsymbol{y}_a^{\ell_a}\right\|_{\Sigma_a}^2 . \tag{20}$$

   and send $(\boldsymbol{A}_{a,b}x_a^{\ell_a+1}, \lambda_{a,b}^{\ell_a})$ to its all neighbors $b \in \mathcal{R}_a$.
2. Wait until n neighbors' $(\boldsymbol{A}_{b,a}x_b^{\ell_a+1}, \lambda_{b,a}^{\ell_a})$.
3. Update $\boldsymbol{y}_a^{\ell_a+1}$ by evaluating

$$\boldsymbol{y}_{a,b}^{\ell_a+1} = \left(\Sigma_a + \Sigma_b\right)^{-1}\left(\Sigma_a\boldsymbol{A}_{b,a}\boldsymbol{x}_b^{\ell_a} + \Sigma_b\boldsymbol{A}_{a,b}\boldsymbol{x}_a^{\ell_a+1} - \lambda_{a,b}^{\ell_a+1} - \lambda_{b,a}^{\ell_a}\right) \tag{21}$$

   for neighbor $b \in \mathcal{R}_a$ associated with arrived information.
4. Update dual by

$$\lambda_a^{\ell_a+1} = \lambda_a^{\ell_a} + \Sigma_a(\boldsymbol{A}_a\boldsymbol{x}_a^{\ell_a+1} - \boldsymbol{y}_a^{\ell_a+1}) . \tag{22}$$

   and set $\ell_a \leftarrow \ell_a + 1$.

Base on the asynchronous framework proposed in [17], Algorithm 1 outlines a tailored asynchronous version of (19) from each area's perspective. Here, we use notation ℓ_a to denote the local iteration counter and $\mathcal{R}_a$ to denote the neighbors of area a. Moreover, we assume that the communication delay is bounded, i.e., all transfer information would eventually arrive at its destination. Compared to the synchronous ADMM, the main idea of Algorithm 1 is to update the consensus variable $\boldsymbol{y}_a$ by using limited neighbors' information. Here, we use $n \le |\mathcal{R}_a|$ in Step (2) of Algorithm 1 to define the number of neighbors whose information are required to proceed the rest steps of Algorithm 1. Notice that these n neighbors whose information is available could be different from iteration to iteration and is dependent on the communication environment. In a result, the consensus variable $\boldsymbol{y}_a$ is not exactly consensus as the local update is only based on the part of neighbors' information. A practical stop criterion of Algorithm 1 is

$$\|\boldsymbol{r}_a^{\ell+1}\|_1 \le \epsilon_a^{\text{pri}} \ , \quad \|\boldsymbol{s}_a^{\ell+1}\|_1 \le \epsilon_a^{\text{dual}}$$

hold for all $a \in \mathcal{R}$ with

$$\epsilon_a^{\text{pri}} = \sqrt{n_{y_a}}\epsilon^{\text{abs}} + \epsilon^{\text{rel}} \max\{\|\boldsymbol{A}_a\boldsymbol{x}_a\|, \|\boldsymbol{y}_a\|\}$$
$$\epsilon_a^{\text{dual}} = \sqrt{n_{x_a}}\epsilon^{\text{abs}} + \epsilon^{\text{rel}}\|\boldsymbol{A}_a^\top\lambda_a\| .$$

Here, the primal and dual residual is given by

$$\boldsymbol{r}_a^{\ell_a+1} = \boldsymbol{A}_a\boldsymbol{x}_a^{\ell_a+1} - \boldsymbol{y}_a^{\ell_a+1} \ , \quad \boldsymbol{s}_a^{\ell_a+1} = \boldsymbol{A}_a^\top\Sigma_a(\boldsymbol{y}_a^{\ell_a+1} - \boldsymbol{y}_a^{\ell_a}),$$

and the parameters ϵ^{abs} and ϵ^{rel} can be chosen as 10^{-3} or 10^{-4} [37]. The primal residual defines the violation of coupled equality constraints (18), while the dual residual describes the residual of the first-order optimality condition of Problem (16). To further explain the main idea of dual residual, we write down the optimality condition of local problem 20 as a generalized equation [38],

$$0 \in \nabla f_a(\boldsymbol{x}_a^{\ell_a+1}) + \boldsymbol{A}_a^\top\lambda_a^{\ell_a} + \boldsymbol{A}_a^\top\Sigma_a\left(\boldsymbol{A}_a\boldsymbol{x}_a^{\ell_a+1} - \boldsymbol{y}_a^{\ell_a}\right) + \mathcal{N}_{\mathcal{X}_a}(\boldsymbol{x}_a^{\ell_a+1})$$

with normal cone $\mathcal{N}_{\mathcal{X}_a}(\boldsymbol{x}_a^{\ell_a+1})$ of constraint set $\mathcal{X}_a$ defined at $\boldsymbol{x}_a^{\ell_a+1}$. Then, substituting the dual update 22 into it yields

$$0 \in \underbrace{\boldsymbol{A}_a^\top\Sigma_a\left(\boldsymbol{y}_a^{\ell_a+1} - \boldsymbol{y}_a^{\ell_a}\right)}_{\text{residual } \boldsymbol{s}_a^{\ell_a+1}} + \underbrace{\nabla f_a(\boldsymbol{x}_a^{\ell_a+1}) + \boldsymbol{A}_a^\top\lambda_a^{\ell_a+1} + \mathcal{N}_{\mathcal{X}_a}(\boldsymbol{x}_a^{\ell_a+1})}_{\text{optimality condition}} .$$

Remark 4 (*Asynchrony and Convergence Guarantee*)**.** Under mild assumptions, Theorem 1 in [39] established the convergence of Algorithm 1 for both iterates and objective value. In practice, one may set $n = 1$ to maximize the communication efficiency, but note that the choice of n does not affect the convergence guarantee as discussed in [39].

Remark 5 (*Step Size*)**.** A proper selection of diagonal matrices Σ_a plays a crucial role in the numerical performance of Algorithm 1. In this paper, for different type of couplings, we choose different diagonal value of Σ_a depending on the magnitude of coupling variables. In particular, there are three different value of $\{20000, 2, 0.002\}$ used for the voltage phase angle of boundary bus in [rad], the pressure of boundary node in [Psig], and the gas flow of tie-pipe in [kcf], respectively.

If there exists a master agent monitoring all the local updates, the iteration of asynchronous ADMM can be also written down from a global point view same as (19). The local primal and dual update is given by

$$\boldsymbol{x}_a^{\ell+1} = \begin{cases} \underset{\boldsymbol{x}_a \in \mathcal{X}_a}{\operatorname{argmin}} f_a(\boldsymbol{x}_a) + \frac{1}{2}\left\|\boldsymbol{A}_a\boldsymbol{x}_a - \boldsymbol{y}_a^{\ell} + \Sigma_a^{-1}\lambda_a^{\ell}\right\|_{\Sigma_a}^2 & \text{if } a \in \mathcal{A}_\ell \\ \boldsymbol{x}_a^{\ell} & \text{otherwise} \end{cases} \tag{23a}$$

$$\lambda_a^{\ell+1} = \begin{cases} \lambda_a^{\ell} + \Sigma_a(\boldsymbol{A}_a\boldsymbol{x}_a^{\ell+1} - \boldsymbol{y}_a^{\ell+1}) & \text{if } a \in \mathcal{A}_\ell \\ \lambda_a^{\ell} & \text{otherwise} \end{cases} \tag{23b}$$

where $\mathcal{A}_\ell \subseteq \mathcal{R}$ is a subset of areas that finishes updating x_a during time interval $(t_\ell, t_{\ell+1}]$. If $\mathcal{A}_v = \mathcal{R}$, (23b) is equivalent to (19a) and (19b). Then, we denote by $T_{(t_\ell, t_{\ell+1}]} \subseteq \mathcal{R} \times \mathcal{R}$ the set of areas that exchange information at iteration ℓ such that the asynchronous update of consensus variable is given by

$$\boldsymbol{y}_{a,b}^{\ell+1} = \left(\Sigma_a + \Sigma_b\right)^{-1}\left(\Sigma_b\boldsymbol{A}_{b,a}\boldsymbol{x}_b^{\ell+1} + \Sigma_a\boldsymbol{A}_{a,b}\boldsymbol{x}_a^{\ell+1} - \lambda_{a,b}^{\ell} - \lambda_{b,a}^{\ell}\right) , \tag{24}$$

for all $(a, b) \in \mathcal{P}$ with $a \in \mathcal{A}_a$.

Fig. 3 shows an example of Algorithm 1 with three workers from the perspective of the master agent that monitors all the local updates (each area is assumed with one worker). Since the workers may have different time delays, the pace of the optimization would be determined by the slowest worker. In Fig. 3(a), the next iteration updates only when all the workers have finished their computation and communication. As a result, under such synchronous protocol, the speedy workers (e.g., worker 1) would spend most of the time idling, and thus the parallel computational resources cannot be fully utilized. Instead, in Fig. 3(b), the next iteration updates whenever at least two workers have finished. With the lock removed, the speedy workers can update their variables more frequently. As illustrated in Fig. 3, during the same period of time, the synchronous algorithm only completes three updates whereas the asynchronous one updates eight times already. On the flip side, the asynchronous one introduces delayed variable information and thereby requires a larger number of iterations to reach the same solution accuracy than its synchronous counterpart. This implies that none of the workers have to be synchronized with each other and does

Table 1
Comparison of synchronous and asynchronous ADMM with centralized method.

Scheme	Iterations	Operation cost ($)			Total operation cost ($)	Solution gap
		Area a	Area b	Area c		
Centralized	–	847223	274668	210474	1332365	–
Synchronous ADMM	51	847241	274679	210487	1332407	0.0030%
Asynchronous ADMM	86	847244	274677	210490	1332411	0.0035%

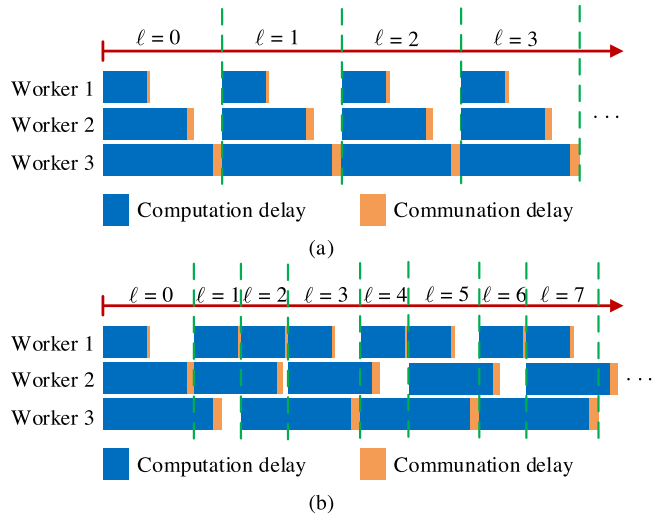

Fig. 3. Illustration of synchronous and asynchronous ADMM (a) Synchronous ADMM, (b) Asynchronous ADMM.

not need to wait for the slowest worker either. In a heterogeneous network, the workers can have different computational powers, or the data sets can be non-uniformly distributed across the network. Thus, the workers can require different computational times in solving the local subproblems. Besides, the communication delays can also be different, e.g., due to probabilistic communication failures and message retransmission.

5. Numerical results

Numerical results are conducted on a three-area 275-bus-130-node IEGS, in which area *a* is comprised of an IEEE 118-bus and a 90-node gas system, area *b* is comprised of an IEEE 118-bus and a 20-node gas system, and area *c* is comprised of a New England 39-bus and a 20-node gas system. Three areas are interconnected by three tie-lines (TLs) and three tie-pipes (TPs) with 14 NGUs, 104 non-NGUs, 13 wind farms, 418 internal lines, 203 electricity loads, 14 gas wells, 6 gas storages, 19 compressors, 117 internal pipelines, and 57 gas loads. The number of wind farms in areas *a*, *b*, and *c* are 5, 5, and 3, respectively. The optimization horizon is 8 h and the time resolution is 1 h. The topology of gas networks can be found in [40]. The parameters of tie-lines and tie-pipes, the unit output characteristics, the electricity and gas network parameters, and other detailed data has been made available online [41]. Variations of wind generation are considered as 20% of their forecasts. The uncertainty budgets of areas *a*, *b*, and *c* are set to 3, 3, and 2, respectively. Initial values of coupling variables and multipliers are all set to zero. The case study is implemented in Matlab R2016a on an Intel Core i5-6500, 3.2 GHz, 16 GB RAM computer. Gurobi 9.0 is used to solve subproblem locally on each core. All local subproblems in synchronous and asynchronous setting are solved using MatlabMPI for parallel processing.

5.1. Comparison of convergence performance and solution quality

We perform benchmarking studies comparing the asynchronous ADMM with its synchronous counterpart to demonstrate its convergence performance. Taking hour 1 as an example, the iteration processes of asynchronous and synchronous ADMM on phase angle of boundary bus, pressure of boundary node are depicted in Fig. 4 and Fig. 5, respectively. The boundary bus angle and boundary node pressure on asynchronous and synchronous ADMM are converged with all the primal and dual residues smaller than the thresholds. The tie-pipe gas flow on hour 1 is selected to compare the relative residue of asynchronous and synchronous ADMM, shown in Fig. 6. As shown from the left column of Fig. 6, the asynchronous and synchronous ADMM converges after 86 and 51 iterations, respectively. As expected, synchronous ADMM takes fewer iterations to converge. This is due to the fact that in asynchronous ADMM a worker uses the most updated information of its neighbors in a more timely manner than in the synchronous case and updates its local variables more frequently, which, as a trade-off, results in more iterations. However, the right column of Fig. 6 shows that the execution time of asynchronous ADMM is much less than synchronous ADMM. We also benchmark the asynchronous and synchronous ADMM with the centralized method to demonstrate comparable solution quality, summarized in Table 1. The operation costs found by the asynchronous and synchronous ADMM are nearly the same as that identified by the centralized method. The solution gap for synchronous and asynchronous ADMM is fairly small.

5.2. Comparison of computation, idle, and execution time

The computation time, idle time, and execution time of asynchronous and synchronous ADMM is demonstrated in Table 2. Noted that the execution time represents the total time that the algorithm takes to converge, including the parallel computation time and idle time. Here, the communication time is not considered as passing message from one worker to the other usually takes a couple of milliseconds using a direct fiber optical link, which is very small compared to local computation time. Thus, there is no idle time for the slowest area *a* in synchronous scheme. In asynchronous scheme, since the computation of area *c* is very fast, once the computation of area *a* or *b* is completed, the next iteration will be performed together with area *c*. Thus, there is no idle time for areas *a* and *b* in asynchronous ADMM. It is clearly shown the asynchronous scheme spends relatively less time idling, while the synchronous scheme suffers from greater amount of idle times. In asynchronous scheme, 26.1% of the time is wasted in idling, while it is 46.6% of the time wasted in idling for synchronous scheme. Although synchronous ADMM takes fewer iterations to converge, the average computation time for one iteration in asynchronous scheme (46 s) is much faster than synchronous scheme (73 s). The execution time of the synchronous ADMM takes 2142 s; whereas the asynchronous ADMM takes 1836 s. Global computational progress in the synchronous scheme is held up by the slowest area *a* which simultaneously incurs very high idle time on the fastest area *c*. Due to the idle time for the slowest worker at each iteration, a lot of time is wasted on waiting for all neighbors using a synchronous scheme. The higher computation time for area *a* form the main bottlenecks for global progress of synchronous scheme which are readily circumvented by asynchronous scheme.

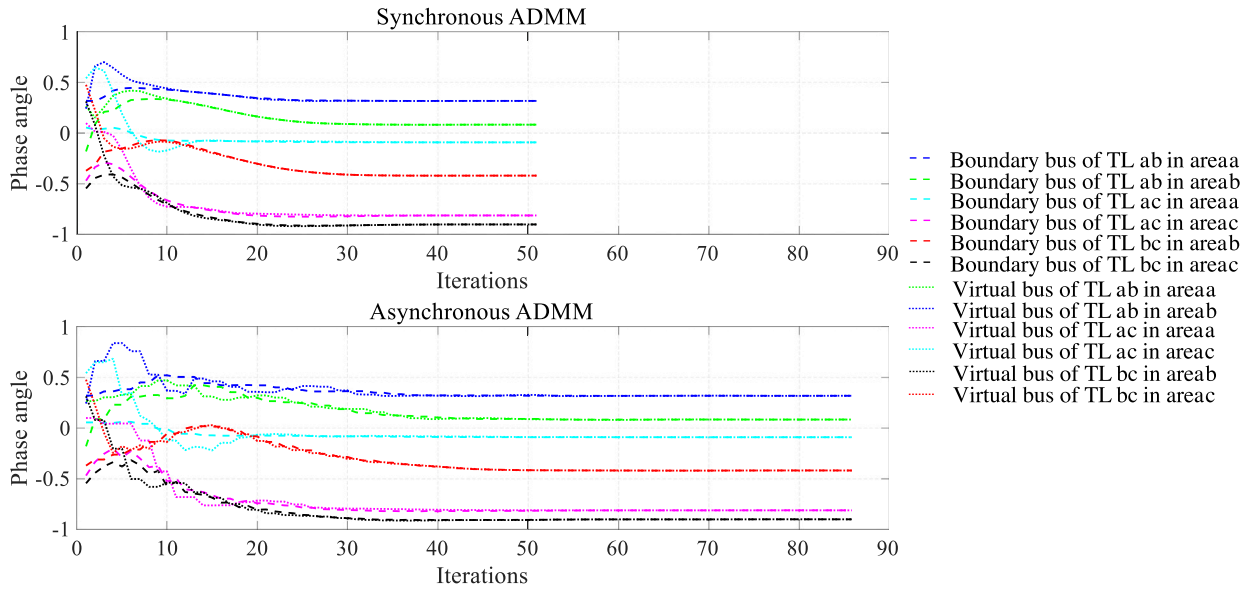

Fig. 4. Convergence curve of boundary bus phase angle.

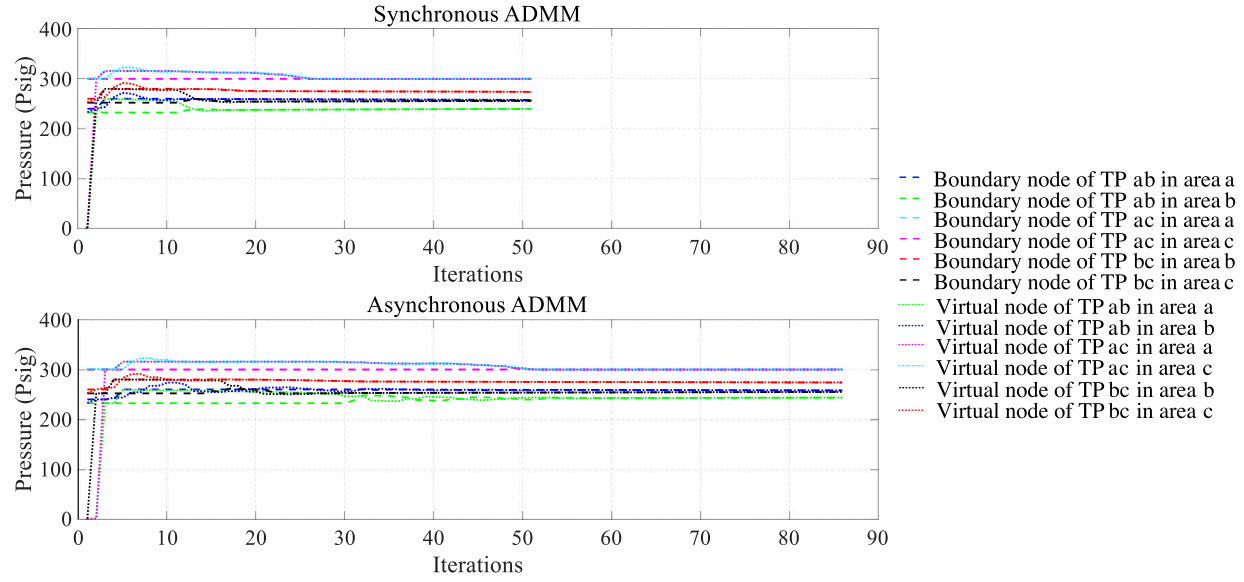

Fig. 5. Convergence curve of boundary node pressure.

Table 2
Comparisons of time for sync. and async. ADMM.

Areas		Syn. ADMM		Asyn. ADMM	
		Time (s)	% of total	Time (s)	% of total
Area *a*	Computation	2105	100.0%	1862	100.0%
	Idle	0	0	0	0
Area *b*	Computation	1476	59.9%	1698	100.0%
	Idle	986	40.1%	0	0
Area *c*	Computation	157	6.5%	427	23.3%
	Idle	2274	93.5%	1408	76.7%
Total	Computation	3738	53.4%	3987	73.9%
	Idle	3260	46.6%	1408	26.1%
Execution		2142	\	1836	\

Despite strongly asynchronous systems, more frequent asynchronous updates are able to successfully drive the problem towards the global solution much faster leading to superior computational efficiency. We can conclude that asynchronous ADMM on average takes more iterations than synchronous ADMM but with less time spent on each iteration. Moreover, for many engineering applications, only a mild level of accuracy is needed. Therefore, asynchronous ADMM generally takes shorter time to converge and the computational efficiency will be further improved in the real applications. Asynchronous ADMM could be more suitable and scalable for the practical deployment and more efficient than its synchronous counterpart. The impact of communication delay on the convergence performance due to information exchange between subsystems will be minimal. The proposed asynchronous scheme is more suitable and scalable for decentralized applications in large-scale multi-area systems. This asynchronous property is more

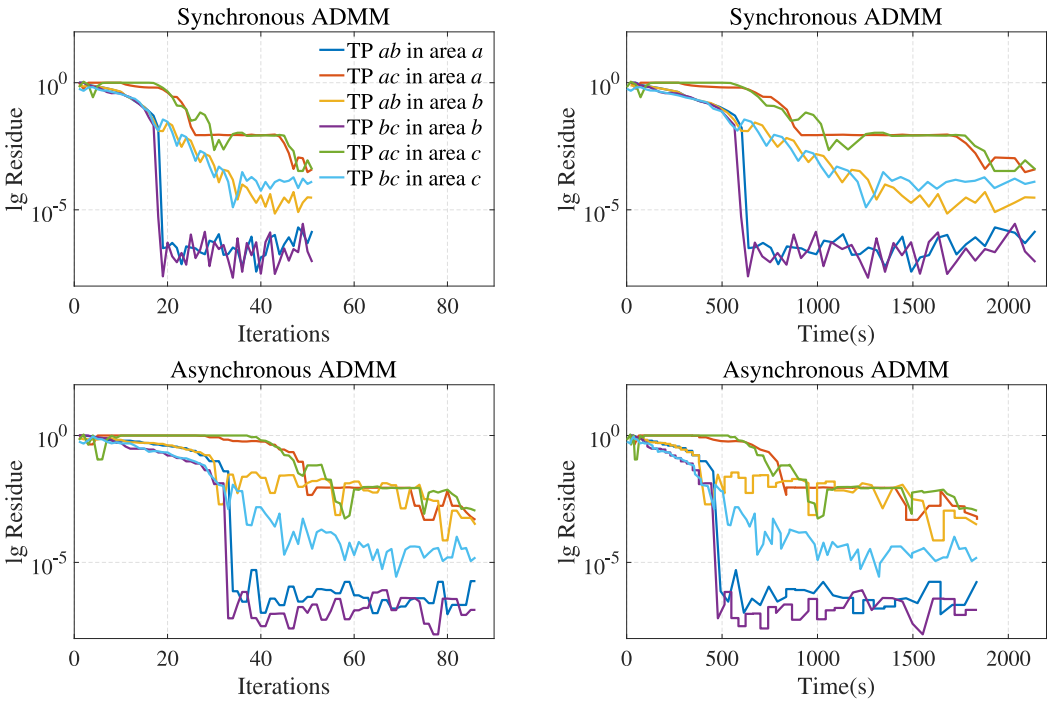

Fig. 6. Convergence of residue on tie-pipe gas flow.

Table 3
Comparison of predefined and optimized AGC participation factors.

σ_a	σ_b	σ_c	Total operation cost ($)	
			Optimized AGC	Predefined AGC
1			1329141	1347592
2			1330553	1348826
3	1	1	1331066	1349012
4			1331601	1351034
5			1332445	1352104

fault-tolerable for delayed or missing information and is invulnerable to communication network condition as well as communication bottleneck.

5.3. Impact of AGC participation factors

Based on the reliability considerations, the traditional AGC participation factors are generally determined according to the generator capacity [42], i.e., $\alpha_g = \overline{P}_g^G / \sum_{g=1}^{\mathcal{G}} \overline{P}_g^G$, so the AGC participation factors are predefined. In order to illustrate the impact of AGC participation factors on solution, we assume that $\sigma_a = \sigma_c = 1$, then the total operation costs of predefined and optimized AGC method with increasing σ_b are compared in Table 3. The predefined AGC refers to the method in [22,23]. We can see that optimizing the AGC participation factors can greatly reduce the total operation cost, meanwhile promote the wind power accommodation. This is because different participation factors correspond to different allocations of wind power among AGC units. In the predefined AGC method, the large-capacity generator has a large participation factor, so its allocated wind power is also large. However, the unit cost for providing the reserve of the large-capacity generator is not necessarily low, which leads to an increase in operation cost.

Additionally, the intention of involving AGC reference output basepoints is to account for how the AGC units will respond to the power mismatch caused by wind power uncertainties, but not to generate signals to control the actual output of AGC units. Output basepoints are provided to AGC units for reference only, and the actual power outputs of these units are ultimately controlled by the AGC system to compensate the area control error. Noted that this proposed LDRs based adjustable robust operation model can simultaneously optimize the AGC participation factors, utilize the budget of uncertainty in a polyhedral uncertainty set, and consider the wind power curtailment situation, which leads to significantly less conservative and more practical solutions.

5.4. Impact of uncertainty budgets

The proposed adjustable robust operation model minimizes the base case generation cost under nominal scenario, while adaptively and securely adjusting the output of AGC units in response to possible realizations of wind power uncertainties. When the budget $\sigma_a = \sigma_b = \sigma_c = 0$, it degenerates into a deterministic optimization problem with no wind power variation. When the budget $\sigma_a = 5$, $\sigma_b = 5$, $\sigma_c = 3$, it degenerates into the nonadjustable bounded interval method in the classical LDRs-based adjustable robust models [24,25], which is the most conservative situation. The operation costs with varying uncertainty budgets are illustrated in Fig. 7. We can see that the total operation cost increases steadily with the increasing uncertainty budget. This is because a larger uncertainty budget corresponds to the more severe wind power fluctuations, which leads to a more conservative solution. This will result in more units generate more energy or consume more gas uneconomically to deal with the worst-case available wind power scenario. By increasing the uncertainty budget, the solution becomes more robust at the expense of higher operation costs. It should be noted that the robust solutions here only reveal the operation cost in the worst-case scenario, the actual solutions can be better than the displayed results.

6. Conclusions

The multi-area IEGS has attracted much attention for its inherent advantages in promoting the energy utilization efficiency. This paper proposes a decentralized optimization method for multi-area IEGS based on asynchronous ADMM that does not require any centralized coordination and allows the control regions to perform local updates

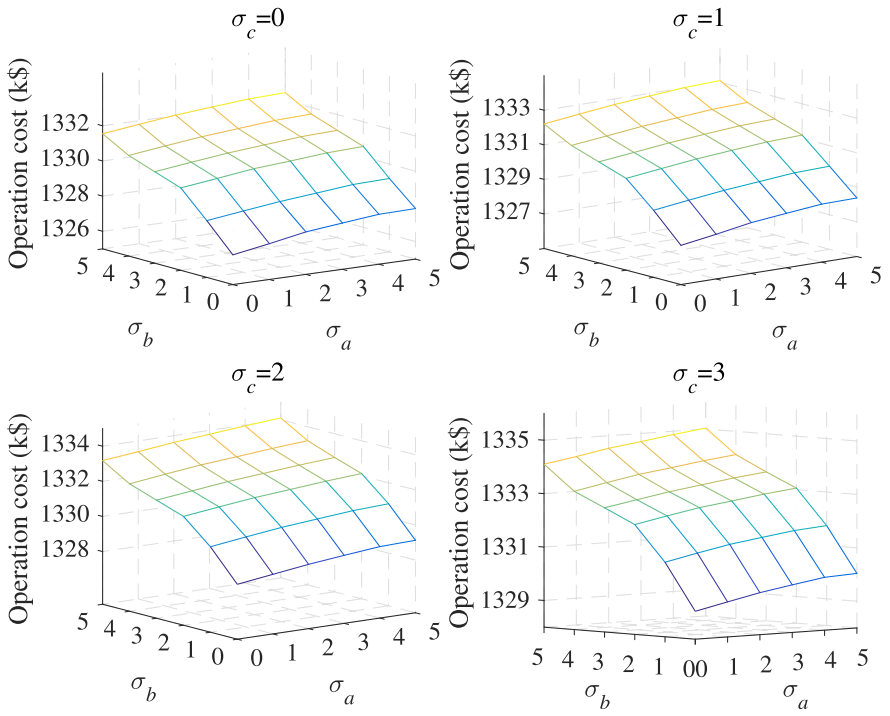

Fig. 7. Total operation cost under different uncertainty budgets.

with information received from a subset of its physically connected neighbors. The LDRs-based adjustable robust extension of asynchronous ADMM capable of handling renewable energy uncertainty is presented, which is coincident with the AGC systems. Using the proposed asynchronous decentralized computing scheme, each IEGSO can operate their respective systems independently and asynchronously, and the information privacy and decision-making independence are preserved.

Future work will investigate several open and more challenging problems, including (1) developing an asynchronous ADMM-based heuristic procedure to consider the discrete decisions (e.g. gas direction) of local IEGS, (2) developing an asynchronous and inexact ADMM algorithm to better adapt to the different complexity of local subsystem, and (3) developing the linear decision rules based adjustable robust model for AC-OPF problem.

CRediT authorship contribution statement

Junyi Zhai: Conceptualization, Software, Investigation, Data curation, Funding acquisition, Writing – original draft. **Yuning Jiang:** Methodology, Validation, Writing – review & editing, Writing – original draft. **Xiao Chen:** Methodology, Writing – review & editing. **Jianing Li:** Formal analysis, Writing – review & editing. **Colin N. Jones:** Supervision, Funding acquisition. **Xiao-Ping Zhang:** Validation, Supervision.

Declaration of competing interest

The authors declare that they have no known competing financial interests or personal relationships that could have appeared to influence the work reported in this paper.

Data availability

Data will be made available on request.

Appendix

(1) *Derivation for unit output constraint*: Substituting (7a) and (7b) into (9e) yields the worst-case robust constraint

$$\hat{P}^G_{gt} - \underline{P}^G_{gt} \geq \alpha_{gt} \cdot \max_{z\in\mathcal{Z}_a} \sum_{k\in\mathcal{W}_a} \left(\tilde{P}^W_{kt} - \overline{P}^W_{kt}\right) \tag{25a}$$

$$\overline{P}^G_{gt} - \hat{P}^G_{gt} \geq \alpha_{gt} \cdot \max_{z\in\mathcal{Z}_a} - \sum_{k\in\mathcal{W}_a} \left(\tilde{P}^W_{kt} - \overline{P}^W_{kt}\right) \tag{25b}$$

for all $g \in \mathcal{G}_a$, $a \in \mathcal{R}$, $t \in \mathcal{T}$. With (5) and (6), the inner maximization problem in (25a) can be equivalently written as:

$$\max_{z\in\mathcal{Z}_a} \sum_{k\in\mathcal{W}_a} \Delta P^W_{kt} \left(z^+_{kt} - z^-_{kt}\right) \tag{26a}$$

$$\text{s.t.} \quad 0 \leq z^+_{kt} \leq 1, \quad k \in \mathcal{W}_a,\ a \in \mathcal{R},\ t \in \mathcal{T} \quad | \ \kappa^{*+}_{gkt} \tag{26b}$$

$$0 \leq z^-_{kt} \leq 1, \quad k \in \mathcal{W}_a,\ a \in \mathcal{R},\ t \in \mathcal{T} \quad | \ \kappa^{*-}_{gkt} \tag{26c}$$

$$z^+_{kt} + z^-_{kt} \leq 1, \quad k \in \mathcal{W}_a,\ a \in \mathcal{R},\ t \in \mathcal{T} \quad | \ \kappa^{*1}_{gkt} \tag{26d}$$

$$\sum_{k\in\mathcal{W}_a} \left(z^+_{kt} + z^-_{kt}\right) \leq \sigma_a,\ a \in \mathcal{R},\ t \in \mathcal{T} \quad | \ \kappa^{*\sigma}_{gt} \tag{26e}$$

Here, κ^{*+}_{gkt}, κ^{*-}_{gkt}, κ^{*1}_{gkt}, and $\kappa^{*\sigma}_{gt}$ represent the dual variables associated with the constraints of uncertainty. In the following, the wild-char superscript is substituted by (Gl), (Gr), (Wl), (Wr), (Vl), (Vr), (Rl), (Rr), and (C) in (27), (28), (29), (30), (40), (41), (44), (45), and (48), respectively. These superscripts are characters only used to discriminate the dual variables. Taking the dual of (26) gives the LDR-based adjustable robust form of (25a) with an uncertainty budget:

$$\hat{P}^G_{gt} - \underline{P}^G_{gt} \geq \sum_{k\in\mathcal{W}_a} \left(\kappa^{(Gl)+}_{gkt} + \kappa^{(Gl)-}_{gkt} + \kappa^{(Gl)1}_{gkt}\right) + \sigma_a \kappa^{(Gl)\sigma}_{gt} \tag{27a}$$

$$\alpha_{gt}\Delta P^W_{kt} \leq \kappa^{(Gl)+}_{gkt} + \kappa^{(Gl)1}_{gkt} + \kappa^{(Gl)\sigma}_{gt} \tag{27b}$$

$$-\alpha_{gt}\Delta P^W_{kt} \leq \kappa^{(Gl)-}_{gkt} + \kappa^{(Gl)1}_{gkt} + \kappa^{(Gl)\sigma}_{gt} \tag{27c}$$

$$\kappa^{(Gl)+}_{gkt} \geq 0,\ \kappa^{(Gl)-}_{gkt} \geq 0,\ \kappa^{(Gl)1}_{gkt} \geq 0,\ \kappa^{(Gl)\sigma}_{gt} \geq 0 \tag{27d}$$

$$\forall k \in \mathcal{W}_a,\ \forall g \in \mathcal{G}_a,\ \forall a \in \mathcal{R},\ \forall t \in \mathcal{T}$$

and similar method can be applied to (25b).

$$\overline{P}^G_{gt} - \hat{P}^G_{gt} \geq \sum_{k\in\mathcal{W}_a} \left(\kappa^{(Gr)+}_{gkt} + \kappa^{(Gr)-}_{gkt} + \kappa^{(Gr)1}_{gkt}\right) + \sigma_a \kappa^{(Gr)\sigma}_{gt} \tag{28a}$$

$$-\alpha_{gt}\Delta P^W_{kt} \leq \kappa^{(Gr)+}_{gkt} + \kappa^{(Gr)1}_{gkt} + \kappa^{(Gr)\sigma}_{gt} \tag{28b}$$

$$\alpha_{gt}\Delta P^W_{kt} \leq \kappa^{(Gr)-}_{gkt} + \kappa^{(Gr)1}_{gkt} + \kappa^{(Gr)\sigma}_{gt} \tag{28c}$$

$$\kappa^{(Gr)+}_{gkt} \geq 0,\ \kappa^{(Gr)-}_{gkt} \geq 0,\ \kappa^{(Gr)1}_{gkt} \geq 0,\ \kappa^{(Gr)\sigma}_{gt} \geq 0 \tag{28d}$$

$$\forall k \in \mathcal{W}_a,\ \forall g \in \mathcal{G}_a,\ \forall a \in \mathcal{R},\ \forall t \in \mathcal{T}$$

(2) *Derivation for wind farm output constraint*: Substituting (7c) into (9d) and using duality theory yielding the LDR-based adjustable form of wind farm output limits as follows:

$$\hat{P}^W_{jt} \geq \sum_{k\in\mathcal{W}_a} \left(\kappa^{(Wl)+}_{jkt} + \kappa^{(Wl)-}_{jkt} + \kappa^{(Wl)1}_{jkt}\right) + \sigma_a \kappa^{(Wl)\sigma}_{jt},\ j \in \mathcal{W}_a \tag{29a}$$

$$\left(\beta_{jkt}+1\right)\Delta P^W_{kt} \leq \kappa^{(Wl)+}_{jkt} + \kappa^{(Wl)1}_{jkt} + \kappa^{(Wl)\sigma}_{jt},\ j = k \tag{29b}$$

$$-\left(\beta_{jkt}+1\right)\Delta P^W_{kt} \leq \kappa^{(Wl)-}_{jkt} + \kappa^{(Wl)1}_{jkt} + \kappa^{(Wl)\sigma}_{jt},\ j = k \tag{29c}$$

$$\beta_{jkt}\Delta P^W_{tk} \leq \kappa^{(Wl)+}_{jkt} + \kappa^{(Wl)1}_{jkt} + \kappa^{(Wl)\sigma}_{jt},\ j \in \mathcal{W}_a, j \neq k \tag{29d}$$

$$-\beta_{jkt}\Delta P^W_{kt} \leq \kappa^{(Wl)-}_{jkt} + \kappa^{(Wl)1}_{jkt} + \kappa^{(Wl)\sigma}_{jt},\ j \in \mathcal{W}_a, j \neq k \tag{29e}$$

$$\kappa^{(Wl)+}_{jkt} \geq 0,\ \kappa^{(Wl)-}_{jkt} \geq 0,\ \kappa^{(Wl)1}_{jkt} \geq 0,\ \kappa^{(Wl)\sigma}_{jt} \geq 0 \tag{29f}$$

$$\forall k \in \mathcal{W}_a,\ \forall a \in \mathcal{R},\ \forall t \in \mathcal{T}$$

and

$$\overline{P}^W_{jt} - \hat{P}^W_{jt} \geq \sum_{k\in\mathcal{W}_a} \left(\kappa^{(Wr)+}_{jkt} + \kappa^{(Wr)-}_{jkt} + \kappa^{(Wr)1}_{jkt}\right) + \sigma_a \kappa^{(Wr)\sigma}_{jt},\ j \in \mathcal{W}_a \tag{30a}$$

$$-\left(\beta_{jkt}+1\right)\Delta P^W_{kt} \leq \kappa^{(Wr)+}_{jkt} + \kappa^{(Wr)1}_{jkt} + \kappa^{(Wr)\sigma}_{jt},\ j = k \tag{30b}$$

$$\left(\beta_{jkt}+1\right)\Delta P^W_{kt} \leq \kappa^{(Wr)-}_{jkt} + \kappa^{(Wr)1}_{jkt} + \kappa^{(Wr)\sigma}_{jt},\ j = k \tag{30c}$$

$$-\beta_{jkt}\Delta P^W_{kt} \leq \kappa^{(Wr)+}_{jkt} + \kappa^{(Wr)1}_{jkt} + \kappa^{(Wr)\sigma}_{jt},\ j \in \mathcal{W}_a, j \neq k \tag{30d}$$

$$\beta_{jkt}\Delta P^W_{kt} \leq \kappa^{(Wr)-}_{jkt} + \kappa^{(Wr)1}_{jkt} + \kappa^{(Wr)\sigma}_{jt},\ j \in \mathcal{W}_a, j \neq k \tag{30e}$$

$$\kappa^{(Wr)+}_{jkt} \geq 0,\ \kappa^{(Wr)-}_{jkt} \geq 0,\ \kappa^{(Wr)1}_{jkt} \geq 0,\ \kappa^{(Wr)\sigma}_{jt} \geq 0 \tag{30f}$$

$$\forall k \in \mathcal{W}_a,\ \forall a \in \mathcal{R},\ \forall t \in \mathcal{T}$$

(3) *Derivation for line flow constraint*: It is desired to derive the LDRs of (9c) and (9g) using the full-set formulation that makes use of the sparse network equations directly in the problem. To this end, the power balance under the realization of wind generation and (7a), (7c) can be writen in matrix format:

$$\boldsymbol{P}^G + \boldsymbol{P}^W - \boldsymbol{B}\theta = \boldsymbol{P}^D \tag{31a}$$

$$\boldsymbol{P}^G = \hat{\boldsymbol{P}}^G - \boldsymbol{\alpha}\left(\boldsymbol{e}^T\boldsymbol{\xi}\right) \tag{31b}$$

$$\boldsymbol{P}^W = \hat{\boldsymbol{P}}^W - \boldsymbol{\beta}\boldsymbol{\xi} \tag{31c}$$

where $\boldsymbol{P}^G$, $\boldsymbol{P}^W$, $\boldsymbol{P}^D$, $\hat{\boldsymbol{P}}^W$, $\hat{\boldsymbol{P}}^G$, and $\boldsymbol{\theta}$ denote matrix of the corresponding quantities, $\boldsymbol{\alpha}$ denotes matrix of adjustable term associate with unit output, $\boldsymbol{\beta}$ denotes matrix of adjustable term associate with wind generation, $\boldsymbol{\xi}$ denotes vector of wind forecast errors, $\boldsymbol{e}$ is a column vector of ones, $\boldsymbol{B}$ is the network admittance matrix. By taking the first bus as the reference bus, the bus angles can be computed as:

$$\boldsymbol{\theta} = \tilde{\boldsymbol{B}}\left(\boldsymbol{P}^G + \boldsymbol{P}^W - \boldsymbol{P}^D\right) \tag{32}$$

where

$$\tilde{\boldsymbol{B}} = \begin{bmatrix} 0 & \boldsymbol{0}_{1\times(n-1)} \\ \boldsymbol{0}_{(n-1)\times 1} & \dot{\boldsymbol{B}}^{-1} \end{bmatrix} \tag{33}$$

and n denote the number of buses in power network, $\dot{\boldsymbol{B}}$ is the sub-matrix obtained from $\boldsymbol{B}$ by removing the first row and column.

Substituting (31c) and (31b) in (32) reveals that the bus angles have two components, $\hat{\boldsymbol{\theta}}$ that represents the non-adjustable term corresponding to the wind forecasts and $\Delta\boldsymbol{\theta}$ that represents the adjustable term varying with the uncertain wind forecast error:

$$\boldsymbol{\theta} = \hat{\boldsymbol{\theta}} + \Delta\boldsymbol{\theta} \tag{34a}$$

$$\hat{\boldsymbol{\theta}} = \tilde{\boldsymbol{B}}\left(\hat{\boldsymbol{P}}^G + \hat{\boldsymbol{P}}^W - \boldsymbol{P}^D\right) \tag{34b}$$

$$\Delta\boldsymbol{\theta} = \tilde{\boldsymbol{B}}\left[-\boldsymbol{\beta}\boldsymbol{\xi} - \boldsymbol{\alpha}\left(\boldsymbol{e}^T\boldsymbol{\xi}\right)\right] \tag{34c}$$

Note that $\tilde{\boldsymbol{B}}$ is a dense matrix while $\boldsymbol{B}$ is sparse in all practical power networks; because the power network should be balanced at any point in time, (34b) that governs the bus angles $\hat{\boldsymbol{\theta}}$ can be equivalently expressed using the elements of the sparse network admittance matrix:

$$\hat{P}^G_{it} + \hat{P}^W_{it} - \sum_{j\in\boldsymbol{\Phi}_i} \frac{\hat{\theta}_{it} - \hat{\theta}_{jt}}{x_{ij}} = P^D_{it},\ \hat{\theta}_1 = 0,\ i \in \mathcal{B}^o_a,\ a \in \mathcal{R},\ t \in \mathcal{T} \tag{35}$$

Expanding (34c) gives

$$\Delta\boldsymbol{\theta} = -\tilde{\boldsymbol{B}}\boldsymbol{\beta}\boldsymbol{\xi} - \tilde{\boldsymbol{B}}\boldsymbol{\alpha}\left(\boldsymbol{e}^T\boldsymbol{\xi}\right) \tag{36}$$

From (36), the change in the angle of bus i due to the uncertain wind forecast error is

$$\begin{aligned}\Delta\theta_{it} &= -\sum_{k\in\mathcal{W}_a} \tilde{B}_{ik}\beta_{ikt}\xi_{kt} - \left(\sum_{g\in\mathcal{G}_a} \tilde{B}_{ig}\alpha_{gt}\right)\sum_{k\in\mathcal{W}_a}\xi_{kt} \\ &= -\sum_{k\in\mathcal{W}_a}\left(\tilde{B}_{ik}\beta_{ikt} + \sum_{g\in\mathcal{G}_a}\tilde{B}_{ig}\alpha_{gt}\right)\xi_{kt}\end{aligned} \tag{37}$$

Similarly, the change in the angle of bus j is

$$\Delta\theta_{jt} = -\sum_{k\in\mathcal{W}_a}\left(\tilde{B}_{jk}\beta_{jkt} + \sum_{g\in\mathcal{G}_a}\tilde{B}_{jg}\alpha_{gt}\right)\xi_{kt} \tag{38}$$

The uncertain power flow in branch ij can be now obtained from (9g), (34a), (37), and (38):

$$\begin{aligned}P_{ijt} &= \frac{1}{x_{ij}}\left(\hat{\theta}_{it} - \hat{\theta}_{jt} + \Delta\theta_{it} - \Delta\theta_{jt}\right) \\ &= \frac{1}{x_{ij}}\left[\hat{\theta}_{it} - \hat{\theta}_{jt} + \sum_{k\in\mathcal{W}_a}\left(\tilde{B}_{jk}\beta_{jkt} - \tilde{B}_{ik}\beta_{ikt} + \sum_{g\in\mathcal{G}_a}\tilde{B}_{jg}\alpha_{gt} - \sum_{g\in\mathcal{G}_a}\tilde{B}_{ig}\alpha_{gt}\right)\xi_{kt}\right].\end{aligned} \tag{39}$$

Similar to the unit and wind farm output limits, with the wind power uncertainty directly included in the branch power flow (39), the LDRs of the line flow limits (9g) is written as the following equivalent set of linear constraints:

$$\overline{L}_{ijt} - \frac{\hat{\theta}_{it} - \hat{\theta}_{jt}}{x_{ij}} \geq \sum_{k\in\mathcal{W}_a}\left(\kappa^{(Vl)+}_{ijkt} + \kappa^{(Vl)-}_{ijkt} + \kappa^{(Vl)1}_{ijkt}\right) + \sigma_a\kappa^{(Vl)\sigma}_{ijt} \tag{40a}$$

$$-\frac{1}{x_{ij}}\left(\tilde{B}_{jk}\beta_{ikt} - \tilde{B}_{ik}\beta_{jkt} - \sum_{g\in\mathcal{G}_a}\tilde{B}_{ig}\alpha_{gt} + \sum_{g\in\mathcal{G}_a}\tilde{B}_{jg}\alpha_{gt}\right)\Delta P^W_{kt} \leq \kappa^{(Vl)+}_{ijkt} + \kappa^{(Vl)1}_{ijkt} + \kappa^{(Vl)\sigma}_{ijt} \tag{40b}$$

$$\frac{1}{x_{ij}}\left(\tilde{B}_{jk}\beta_{ikt} - \tilde{B}_{ik}\beta_{jkt} - \sum_{g\in\mathcal{G}_a}\tilde{B}_{ig}\alpha_{gt} + \sum_{g\in\mathcal{G}_a}\tilde{B}_{jg}\alpha_{gt}\right)\Delta P^W_{kt} \leq \kappa^{(Vl)-}_{ijkt} + \kappa^{(Vl)1}_{ijkt} + \kappa^{(Vl)\sigma}_{ijt} \tag{40c}$$

$$\kappa^{(Vl)+}_{ijkt} \geq 0, \kappa^{(Vl)-}_{ijkt} \geq 0, \kappa^{(Vl)1}_{ijkt} \geq 0, \kappa^{(Vl)\sigma}_{ijt} \geq 0 \tag{40d}$$

$$\forall k \in \mathcal{W}_a, \forall (i,j) \in \mathcal{L}_a, \forall a \in \mathcal{R}, \forall t \in \mathcal{T}$$

and

$$\bar{L}_{ijt} + \frac{\hat{\theta}_{it} - \hat{\theta}_{jt}}{x_{ij}} \geq \sum_{k\in\mathcal{W}_a}\left(\kappa^{(Vr)+}_{ijkt} + \kappa^{(Vr)-}_{ijkt} + \kappa^{(Vr)1}_{ijkt}\right) + \sigma_a\kappa^{(Vr)\sigma}_{ijt} \tag{41a}$$

$$\frac{1}{x_{ij}}\left(\tilde{B}_{jk}\beta_{ikt} - \tilde{B}_{ik}\beta_{jkt} - \sum_{g\in\mathcal{G}_a}\tilde{B}_{ig}\alpha_{gt} + \sum_{g\in\mathcal{G}_a}\tilde{B}_{jg}\alpha_{gt}\right)$$

$$\Delta P_{kt}^{W} \le \kappa_{ijkt}^{(Vr)+} + \kappa_{ijkt}^{(Vr)1} + \kappa_{ijt}^{(Vr)\sigma} \tag{41b}$$

$$-\frac{1}{x_{ij}}\left(\tilde{B}_{jk}\beta_{ikt} - \tilde{B}_{ik}\beta_{jkt} - \sum_{g\in\mathcal{G}_a}\tilde{B}_{ig}\alpha_{gt} + \sum_{g\in\mathcal{G}_a}\tilde{B}_{jg}\alpha_{gt}\right)$$

$$\Delta P_{kt}^{W} \le \kappa_{ijkt}^{(Vr)-} + \kappa_{ijkt}^{(Vr)1} + \kappa_{ijt}^{(Vr)\sigma} \tag{41c}$$

$$\kappa_{ijkt}^{(Vr)+} \ge 0, \kappa_{ijkt}^{(Vr)-} \ge 0, \kappa_{ijkt}^{(Vr)1} \ge 0, \kappa_{ijt}^{(Vr)\sigma} \ge 0 \tag{41d}$$

$$\forall k \in \mathcal{W}_a, \forall (i,j) \in \mathcal{L}_a, \forall a \in \mathcal{R}, \forall t \in \mathcal{T}$$

(4) *Derivation for unit ramping rate constraint*: Substituting (7a) and (7b) into (9f) yields the worst-case robust unit ramping rate constraint

$$\hat{P}_{gt}^{G} - \hat{P}_{gt-1}^{G} + R_g^{D} \ge \max_{z\in\mathcal{Z}_a}\left\{\alpha_{gt}\sum_{k\in\mathcal{W}_a}\left(\tilde{P}_{kt}^{W} - \overline{P}_{kt}^{W}\right) - \alpha_{gt-1}\sum_{k\in\mathcal{W}_a}\left(\tilde{P}_{kt-1}^{W} - \overline{P}_{kt-1}^{W}\right)\right\} \tag{42a}$$

$$-\hat{P}_{gt}^{G} + \hat{P}_{gt-1}^{G} + R_g^{U} \ge \max_{z\in\mathcal{Z}_a}\left\{-\alpha_{gt}\sum_{k\in\mathcal{W}_a}\left(\tilde{P}_{kt}^{W} - \overline{P}_{kt}^{W}\right) + \alpha_{gt-1}\sum_{k\in\mathcal{W}_a}\left(\tilde{P}_{kt-1}^{W} - \overline{P}_{kt-1}^{W}\right)\right\} \tag{42b}$$

for all $g \in \mathcal{G}_a$, $a \in \mathcal{R}$, $t \in \mathcal{T}\backslash\{1\}$. The inner maximization problem in (42a) can be equivalently written as:

$$\max_{z\in\mathcal{Z}_a}\left\{\alpha_{gt}\sum_{k\in\mathcal{W}_a}\Delta P_{kt}^{W}\left(z_{kt}^{+} - z_{kt}^{-}\right) - \alpha_{gt-1}\sum_{k\in\mathcal{W}_a}\Delta P_{kt-1}^{W}\left(z_{kt-1}^{+} - z_{kt-1}^{-}\right)\right\} \tag{43a}$$

$$\text{s.t.} \quad 0 \le z_{kt}^{+} \le 1, \quad k \in \mathcal{W}_a,\ a \in \mathcal{R},\ t \in \mathcal{T}\backslash\{1\} \quad | \ \kappa_{gkt}^{*+} \tag{43b}$$

$$0 \le z_{kt}^{-} \le 1, \quad k \in \mathcal{W}_a,\ a \in \mathcal{R},\ t \in \mathcal{T}\backslash\{1\} \quad | \ \kappa_{gkt}^{*-} \tag{43c}$$

$$z_{kt}^{+} + z_{kt}^{-} \le 1, \quad k \in \mathcal{W}_a,\ a \in \mathcal{R},\ t \in \mathcal{T}\backslash\{1\} \quad | \ \kappa_{gkt}^{*1} \tag{43d}$$

$$\sum_{k\in\mathcal{W}_a}\left(z_{kt}^{+} + z_{kt}^{-}\right) \le \sigma_a,\ a \in \mathcal{R},\ t \in \mathcal{T}\backslash\{1\} \quad | \ \kappa_{gt}^{*\sigma} \tag{43e}$$

$$0 \le z_{kt-1}^{+} \le 1, \quad k \in \mathcal{W}_a,\ a \in \mathcal{R},\ t \in \mathcal{T}\backslash\{1\} \quad | \ \kappa_{gkt-1}^{*+} \tag{43f}$$

$$0 \le z_{kt-1}^{-} \le 1, \quad k \in \mathcal{W}_a,\ a \in \mathcal{R},\ t \in \mathcal{T}\backslash\{1\} \quad | \ \kappa_{gkt-1}^{*-} \tag{43g}$$

$$z_{kt-1}^{+} + z_{kt-1}^{-} \le 1, \quad k \in \mathcal{W}_a,\ a \in \mathcal{R},\ t \in \mathcal{T}\backslash\{1\} \quad | \ \kappa_{gkt-1}^{*1} \tag{43h}$$

$$\sum_{k\in\mathcal{W}_a}\left(z_{kt-1}^{+} + z_{kt-1}^{-}\right) \le \sigma_a,\ a \in \mathcal{R},\ t \in \mathcal{T}\backslash\{1\} \quad | \ \kappa_{gt-1}^{*\sigma} \tag{43i}$$

Taking the dual of (43) gives the LDR-based adjustable robust form of (42a) with an uncertainty budget:

$$\hat{P}_{gt}^{G} - \hat{P}_{gt-1}^{G} + R_g^{D} \ge \sum_{k\in\mathcal{W}_a}\left(\kappa_{gkt}^{(Rl)+} + \kappa_{gkt}^{(Rl)-} + \kappa_{gkt}^{(Rl)1}\right) + \sigma_a\kappa_{gt}^{(Rl)\sigma} + \sum_{k\in\mathcal{W}_a}\left(\kappa_{gkt-1}^{(Rl)+} + \kappa_{gkt-1}^{(Rl)-} + \kappa_{gkt-1}^{(Rl)1}\right) + \sigma_a\kappa_{gt-1}^{(Rl)\sigma} \tag{44a}$$

$$\alpha_{gt}\Delta P_{kt}^{W} - \alpha_{gt-1}\Delta P_{kt-1}^{W} \le \kappa_{gkt}^{(Rl)+} + \kappa_{gkt}^{(Rl)1} + \kappa_{gt}^{(Rl)\sigma} + \kappa_{gkt-1}^{(Rl)+} + \kappa_{gkt-1}^{(Rl)1} + \kappa_{gt-1}^{(Rl)\sigma} \tag{44b}$$

$$-\alpha_{gt}\Delta P_{kt}^{W} + \alpha_{gt-1}\Delta P_{kt-1}^{W} \le \kappa_{gkt}^{(Rl)-} + \kappa_{gkt}^{(Rl)1} + \kappa_{gt}^{(Rl)\sigma} + \kappa_{gkt-1}^{(Rl)-} + \kappa_{gkt-1}^{(Rl)1} + \kappa_{gt-1}^{(Rl)\sigma} \tag{44c}$$

$$\kappa_{gkt}^{(Rl)+} \ge 0,\ \kappa_{gkt}^{(Rl)-} \ge 0,\ \kappa_{gkt}^{(Rl)1} \ge 0,\ \kappa_{gt}^{(Rl)\sigma} \ge 0 \tag{44d}$$

$$\forall k \in \mathcal{W}_a,\ \forall g \in \mathcal{G}_a,\ \forall a \in \mathcal{R},\ t \in \mathcal{T}\backslash\{1\}$$

and similar method can be applied to (42b).

$$-\hat{P}_{gt}^{G} + \hat{P}_{gt-1}^{G} + R_g^{U} \ge \sum_{k\in\mathcal{W}_a}\left(\kappa_{gkt}^{(Rr)+} + \kappa_{gkt}^{(Rr)-} + \kappa_{gkt}^{(Rr)1}\right) + \sigma_a\kappa_{gt}^{(Rr)\sigma} + \sum_{k\in\mathcal{W}_a}\left(\kappa_{gkt-1}^{(Rr)+} + \kappa_{gkt-1}^{(Rr)-} + \kappa_{gkt-1}^{(Rr)1}\right) + \sigma_a\kappa_{gt-1}^{(Rr)\sigma} \tag{45a}$$

$$-\alpha_{gt}\Delta P_{kt}^{W} + \alpha_{gt-1}\Delta P_{kt-1}^{W} \le \kappa_{gkt}^{(Rr)+} + \kappa_{gkt}^{(Rr)1} + \kappa_{gt}^{(Rr)\sigma} + \kappa_{gkt-1}^{(Rr)+} + \kappa_{gkt-1}^{(Rr)1} + \kappa_{gt-1}^{(Rr)\sigma} \tag{45b}$$

$$\alpha_{gt}\Delta P_{kt}^{W} - \alpha_{gt-1}\Delta P_{kt-1}^{W} \le \kappa_{gkt}^{(Rr)-} + \kappa_{gkt}^{(Rr)1} + \kappa_{gt}^{(Rr)\sigma} + \kappa_{gkt-1}^{(Rr)-} + \kappa_{gkt-1}^{(Rr)1} + \kappa_{gt-1}^{(Rr)\sigma} \tag{45c}$$

$$\kappa_{gkt}^{(Rr)+} \ge 0,\ \kappa_{gkt}^{(Rr)-} \ge 0,\ \kappa_{gkt}^{(Rr)1} \ge 0,\ \kappa_{gt}^{(Rr)\sigma} \ge 0 \tag{45d}$$

$$\forall k \in \mathcal{W}_a,\ \forall g \in \mathcal{G}_a,\ \forall a \in \mathcal{R},\ t \in \mathcal{T}\backslash\{1\}$$

(5) *Derivation for electricity and gas coupling constraint*: The electricity and natural gas coupling constraint (10r) can be directly converted into the following form, which is always tight since the unnecessary natural gas consumption by NGUs will lead to higher operation costs.

$$F_{it}^{G} \ge \omega_g P_{gt}^{G},\ (i,g) \in \Omega_a,\ a \in \mathcal{R},\ t \in \mathcal{T} \tag{46}$$

Substituting (7a) and (7b) into (46) yields the worst possible inequality

$$F_{it}^{G} - \omega_g\hat{P}_{gt}^{G} \ge \omega_g\alpha_{gt}\cdot\max_{z\in\mathcal{Z}_a} -\sum_{k\in\mathcal{W}_a}\left(\tilde{P}_{kt}^{W} - \overline{P}_{kt}^{W}\right),\ (i,g) \in \Omega_a,\ a \in \mathcal{R},\ t \in \mathcal{T} \tag{47}$$

Using the duality of (26), the LDRs-based adjustable robust form of (47) can be derived as

$$F_{it}^{G} - \omega_g\hat{P}_{gt}^{G} \ge \sum_{k\in\mathcal{W}_a}\left(\kappa_{gkt}^{(C)+} + \kappa_{gkt}^{(C)-} + \kappa_{gkt}^{(C)1}\right) + \sigma_a\kappa_{gt}^{(C)\sigma} \tag{48a}$$

$$-\omega_g\alpha_{gt}\Delta P_{kt}^{W} \le \kappa_{gkt}^{(C)+} + \kappa_{gkt}^{(C)1} + \kappa_{gt}^{(C)\sigma} \tag{48b}$$

$$\omega_g\alpha_{gt}\Delta P_{kt}^{W} \le \kappa_{gkt}^{(C)-} + \kappa_{gkt}^{(C)1} + \kappa_{gt}^{(C)\sigma} \tag{48c}$$

$$\kappa_{gkt}^{(C)+} \ge 0,\ \kappa_{gkt}^{(C)-} \ge 0,\ \kappa_{gkt}^{(C)1} \ge 0,\ \kappa_{gt}^{(C)\sigma} \ge 0 \tag{48d}$$

$$\forall k \in \mathcal{W}_a, \forall (i,g) \in \Omega_a, \forall a \in \mathcal{R}, \forall t \in \mathcal{T}$$

References

[1] Chen J, Lin Z, Ren J, Zhang W, Zhou Y, Zhang Y. Distributed multi-scenario optimal sizing of integrated electricity and gas system based on ADMM. Int J Electr Power Energy Syst 2020;117:105675.

[2] Zhai J, Wang S, Guo L, Jiang Y, Kang Z, Jones CN. Data-driven distributionally robust joint chance-constrained energy management for multi-energy microgrid. Appl Energy 2022;326:119939.

[3] Feng C, Liang B, Li Z, Liu W, Wen F. Peer-to-peer energy trading under network constraints based on generalized fast dual ascent. IEEE Trans Smart Grid 2022;1.

[4] Borrazsanchez C, Bent R, Backhaus S, Hijazi H, Van Hentenryck P. Convex relaxations for gas expansion planning. INFORMS J Comput 2016;28(4):645–56.

[5] Huang H, Zhang A, Xu X, Li Q, Yang W, Qu G. Optimal scheduling of bidirectional coupled electricity-natural gas systems based on multi-port gas network equivalent model. Int J Electr Power Energy Syst 2022;139:108049.

[6] Zhejing B, Yangli Y, Lei W. Multi-timescale coordinated schedule of interdependent electricity-natural gas systems considering electricity grid steady-state and gas network dynamics. Int J Electr Power Energy Syst 2020;118:105763.

[7] Qi F, Shahidehpour M, Wen F, Li Z, He Y, Yan M. Decentralized privacy-preserving operation of multi-area integrated electricity and natural gas systems with renewable energy resources. IEEE Trans Sustain Energy 2020;11(3):1785–96.

[8] Zhai J, Jiang Y, Li J, Jones C, Zhang X-P. Distributed adjustable robust optimal power-gas flow considering wind power uncertainty. Int J Electr Power Energy Syst 2022;139.

[9] Zhai J, Zhou M, Li J, Zhang X-P, Li G, Ni C, et al. Hierarchical and robust scheduling approach for VSC-MTDC meshed AC/DC grid with high share of wind power. IEEE Trans Power Syst 2021;36(1):793–805.

[10] Zhou M, Zhai J, Li G, Ren J. Distributed dispatch approach for bulk AC/DC hybrid systems with high wind power penetration. IEEE Trans Power Syst 2018;33(3):3325–36.

[11] Zhai J, Dai X, Jiang Y, Xue Y, Hagenmeyer V, Jones CN, et al. Distributed optimal power flow for VSC-MTDC meshed AC/DC grids using ALADIN. IEEE Trans Power Syst 2022;37(6):4861–73.

[12] Zhai J, Jiang Y, Shi Y, Jones CN, Zhang X-P. Distributionally robust joint chance-constrained dispatch for integrated transmission-distribution systems via distributed optimization. IEEE Trans Smart Grid 2022;13(3):2132–47.

[13] Liu C, Wang J, Fu Y, Koritarov V. Multi-area optimal power flow with changeable transmission topology. IET Gener Transm Distrib 2014;8(6):1082–9.

[14] Li Z, Guo Q, Sun H, Wang J. Coordinated economic dispatch of coupled transmission and distribution systems using heterogeneous decomposition. IEEE Trans Power Syst 2016;31(6):4817–30.

[15] Bakirtzis AG, Biskas PN. A decentralized solution to the DC-OPF of interconnected power systems. IEEE Trans Power Syst 2003;18(3):1007–13.

[16] Lin C, Wu W, Zhang B, Wang B, Zheng W, Li Z. Decentralized reactive power optimization method for transmission and distribution networks accommodating large-scale DG integration. IEEE Trans Sustain Energy 2017;8(1):363–73.
[17] Guo J, Hug G, Tonguz O. Impact of communication delay on asynchronous distributed optimal power flow using ADMM. In: 2017 IEEE international conference on smart grid communications. 2017, p. 177–82.
[18] Ramanan P, Yildirim M, Chow E, Gebraeel N. An asynchronous, decentralized solution framework for the large scale unit commitment problem. IEEE Trans Power Syst 2019;34(5):3677–86.
[19] Zhang Y, Yang J, Pan X, Zhu X, Liu S. Data-driven robust dispatch for integrated electric-gas system considering the correlativity of wind-solar output. Int J Electr Power Energy Syst 2022;134(3):107454.
[20] Li Z, Shahidehpour M, Wu W, Zeng B, Zhang B, Zheng W. Decentralized multiarea robust generation unit and tie-line scheduling under wind power uncertainty. IEEE Trans Sustain Energy 2015;6(4):1377–88.
[21] Li Z, Wu W, Shahidehpour M, Zhang B. Adaptive robust tie-line scheduling considering wind power uncertainty for interconnected power systems. IEEE Trans Power Syst 2016;31(4):2701–13.
[22] Li Z, Wu W, Zhang B, Wang B. Adjustable robust real-time power dispatch with large-scale wind power integration. IEEE Trans Sustain Energy 2015;6(2):357–68.
[23] Zhao J, Zheng T, Litvinov E. Variable resource dispatch through do-not-exceed limit. IEEE Trans Power Syst 2015;30(2):820–8.
[24] Jabr RA, Karaki S, Korbane JA. Robust multi-period OPF with storage and renewables. IEEE Trans Power Syst 2015;30(5):2790–9.
[25] Jabr RA. Adjustable robust OPF with renewable energy sources. IEEE Trans Power Syst 2013;28(4):4742–51.
[26] Attarha A, Scott P, Thiébaux S. Affinely adjustable robust ADMM for residential DER coordination in distribution networks. IEEE Trans Smart Grid 2020;11(2):1620–9.
[27] Dehghan S, Amjady N, Conejo AJ. Adaptive robust transmission expansion planning using linear decision rules. IEEE Trans Power Syst 2017;32(5):4024–34.
[28] Bertsimas D, Litvinov E, Sun XA, Zhao J, Zheng T. Adaptive robust optimization for the security constrained unit commitment problem. IEEE Trans Power Syst 2013;28(1):52–63.
[29] Wang C, Wei W, Wang J, Bi T. Convex optimization based adjustable robust dispatch for integrated electric-gas systems considering gas delivery priority. Appl Energy 2019;239(APR.1):70–82.
[30] Sánchez CB, Bent R, Backhaus S, Blumsack S, Hijazi H, van Hentenryck P. Convex optimization for joint expansion planning of natural gas and power systems. In: 2016 49th Hawaii international conference on system sciences. HICSS, 2016, p. 2536–45.
[31] Keyaerts N. Gas balancing and line-pack flexibility. Concepts and methodologies for organizing and regulating gas balancing in liberalized and integrated EU gas markets. 2012.
[32] Chen S, Conejo AJ, Sioshansi R, Wei Z. Unit commitment with an enhanced natural gas-flow model. IEEE Trans Power Syst 2019;34(5):3729–38.
[33] Chen S, Wei Z, Sun G, Cheung KW, Wang D. Identifying optimal energy flow solvability in electricity-gas integrated energy systems. IEEE Trans Sustain Energy 2017;8(2):846–54.
[34] Qadrdan M, Wu J, Jenkins N, Ekanayake J. Operating strategies for a GB integrated gas and electricity network considering the uncertainty in wind power forecasts. IEEE Trans Sustain Energy 2014;5(1):128–38.
[35] Wen Y, Qu X, Li W, Liu X, Ye X. Synergistic operation of electricity and natural gas networks via ADMM. IEEE Trans Smart Grid 2018;9(5):4555–65.
[36] Li Y, Li Z, Wen F, Shahidehpour M. Minimax-regret robust co-optimization for enhancing the resilience of integrated power distribution and natural gas systems. IEEE Trans Sustain Energy 2020;11(1):61–71.
[37] Boyd S, Parikh N, Chu E, Peleato B, Eckstein J. Distributed optimization and statistical learning via the alternating direction method of multipliers. Found Trends® Mach Learn 2011;3(1):1–122.
[38] Boyd S, Boyd SP, Vandenberghe L. Convex optimization. Cambridge University Press; 2004.
[39] Guo J, Hug G, Tonguz O. Asynchronous ADMM for distributed non-convex optimization in power systems. 2017, arXiv preprint arXiv:1710.08938.
[40] Yang L, Xu Y, Sun H, Zhao X. Two-stage convexification-based optimal electricity-gas flow. IEEE Trans Smart Grid 2020;11(2):1465–75.
[41] https://github.com/JunyiZhai1990/Multi-area-IEGS.
[42] Wei W, Liu F, Mei S. Dispatchable region of the variable wind generation. IEEE Trans Power Syst 2015;30(5):2755–65.